Different Data, Different General Circulations? A Comparison of Selected Fields in NCEP/DOE AMIP-II and ECMWF ERA-40 Reanalyses

by

Richard Grotjahn

Department of Land, Air, and Water Resources,
University of California, Davis, 95616, U.S.A.

Submitted 6 March 2006
Revised April 2007

A submission for a special issue
of *Dynamics of Atmospheres and Oceans*
Current Contributions to Understanding the General Circulation of the Atmosphere
Part 2

Abstract

Reanalysis datasets have been very popular for understanding the general circulation as well as verifying general circulation models. The most recent versions of global reanalysis datasets prepared by ECMWF ("ERA-40") and NCEP ("NDRa2") are examined in this article. The NDRa2 data are regridded to the resolution (2.5 by 2.5 degrees longitude and latitude) of the ERA-40 public data. Primary variables that both relate to the atmosphere's general circulation and are readily available are compared and contrasted. Significant differences are found in the primary circulation variables and energetics. The subtropical and polar night jet streams are stronger in ERA-40 data as is kinetic energy. The surface energy budgets differ in that ERA-40 data have greater sensible heat flux into the air, while NDRa2 data have greater latent heat flux. The result is NDRa2 has more moisture in the subtropics; ERA-40 data have more moisture in the tropics. Geographically, the two datasets have notable differences in their treatment of the intertropical convergence zone (ICZ). The ICZ over the Atlantic and eastern Pacific is narrower and stronger in ERA-40 data. The ICZ over the western Pacific and Indian oceans is generally stronger in NDRa2 data, one consequence is a stronger tropical easterly jet in NDRa2 data over the Indian Ocean in JJA. Both datasets have a double ICZ in the western half of the Pacific in DJF; in JJA ERA-40 retains that double ICZ but NDRa2 largely does not. Beyond the handling of the ICZ, the datasets differ in tropical zonal mean zonal wind, ERA-40 data in DJF has zonal mean upper troposphere tropical westerlies where NDRa2 data have easterlies; this difference may imply a different amount of interhemispheric communication. The datasets also have strong disagreements in regions of large-scale higher topography.

1. Introduction

The large scale patterns of two popular 'reanalysis' datasets are compared. An 'analysis' is a dataset created by an 'assimilation system'. A 'reanalysis' uses the same assimilation system to process the entire record. The purpose is to improve the statistical uniformity of each dataset, but uniformity is not guaranteed because the observations available evolve over the record.

In recent years operational centers at the European Centre for Medium Range Weather Forecasts (ECMWF) and the U.S. National Center for Environmental Prediction (NCEP) have made a huge effort to produce uniform, long period reanalysis datasets. (Abbreviations and acronyms are defined in an appendix.) The initial, widely used data sets are "ERA15": a 15 year climatology from December 1978 through February 1994 produced by ECMWF and "NNRa1": the NCEP-NCAR Reanalysis, a climatology starting from January 1948. NNRa1 was improved upon by the NCEP-DOE AMIP-II Reanalysis dataset, "NDRa2" covering the period starting from January 1979 as of this writing. These 'first generation' datasets have been succeeded by a newer dataset: "ERA-40": an ECMWF dataset covering the 45 year period from September 1957 through August 2002.

Uppalla et al. (2005) discuss various properties of ERA-40 including how it builds upon ERA15. The assimilation system for ERA-40 differs from ERA15 by using a three dimensional variational data assimilation scheme. Table 1 has a summary of the observations used by ERA-40. Table 2 summarizes the ERA-40 assimilation model properties. The ERA-40 assimilation system is similar to the system used operationally at ECMWF in the latter half of 2001. One may compare Tables 1 and 2 with a table showing corresponding observational inputs and properties of ERA15 presented by Hodges et al. (2003). ERA-40 uses significantly more observations and types of observations than ERA15 and assimilates them differently. Uppala et al. emphasize a 'more comprehensive use of satellite data' than was the case for ERA15. ERA-40 directly assimilated raw radiance data, not just retrievals. Other data (scatterometer and SSM/I)

were directly assimilated when available. ERA-40 included significant level radiosonde data (unlike ERA15). Uppala et al. (2005, p. 2963) list some deficiencies present in ERA15 that were corrected by ERA-40. Despite considerable improvement over ERA15, Uppala et al. (2005) discuss two primary deficiencies in ERA-40 data: excessive tropical precipitation (due to the model adjusting to its dry bias) and too strong of a stratospheric 'Brewer-Dobson' circulation. More is said about the moisture bias in section 2.5.

The NNRa1 data are described by Kalnay et al. (1996) and Kistler et al. (2001). The revised reanalysis NDRa2 is described by Kanamitsu et al. (2002). Kanamitsu do not represent the NDRa2 data as a 'second generation' product, but as an improvement of deficiencies identified in the NNRa1 data. Kanamitsu et al. include a list of deficiencies corrected by NDRa2. Observations incorporated into the NDRa2 reanalysis are summarized in Table 1. Properties of the NDRa2 assimilation system are summarized in Table 2. *When comparing the observations (Table 1) and assimilation system (Table 2) it is clear that ERA-40 is intended to capture more observational information than NDRa2. While NDRa2 does not extend as far back in time as ERA-40, the NDRa2 record presently continues into the future.*

Despite a fixed assimilation system, the evolving observational network can make the data record inhomogeneous. Perhaps the largest change in the past 60 years occurs before and after the advent of large amounts of satellite data. Different forms of satellite data were introduced over many years: infrared satellite and PAOBS data begin in 1973; MSU, TOMS ozone, and cloud-tracked winds data begin around 1979; TCWV begins around 1987; ocean wave data from around 1991. It is well known that the NNRa1 climatology of the NCEP dataset is noticeably different before and after 1978 (e.g. Kistler, et al, 2001, p. 252; Trenberth and Smith, 2005). Analysis increments (differences between 6 or 12 hour forecasts and subsequent analyses) decreases can imply analysis improvements (except when the observations are too sparse). Kistler et al. (2001) show analysis increments time series for NNRa1 while Uppala et al. (2005) show analysis increments time series for ERA-40; in both datasets the advent of the satellite data makes a big improvement. For example: Uppala et al. (2005, p. 2982-3) show global average

surface pressure to fluctuate less after 1973 and less still after 1979. Sterl (2004) show SLP and 500 hPa Z (geopotential height) differences between ERA-40 and NNRa1 diminish markedly after 1978. Trenberth and Smith (2005) show global surface pressure variation changing dramatically from large before to small after 1979. Simmons et al. (2004) show differences of two meter temperature (T) between NNRa1 and ERA-40 that diminish noticeably, starting around the late 1970's. Bromwich and Fogt (2004) find stunning improvement in SLP, two meter T, and 500 hPa Z after 1978 at middle and high latitudes of the Southern Hemisphere. Hagemann et al. (2005) detail changes in elements of ERA-40's hydrological cycle before, during, and after the transition to a full suite of satellite data. The most dramatic improvements in the satellite network occurred as activity ramped up for the Global Weather Experiment (GWE) beginning around December 1978. *For these reasons this report will focus only on the satellite era, restricting attention to data starting after December 1978.* Since different models, different observations, and objective analysis techniques were used at ECMWF and NCEP, the reanalysis datasets are not the same even though many of the observations input are the same. There is some evidence (Renwick, 2003) that the differences between ERA-40 and NNRa1, for at least some variables, is less after 1979 as well.

The data are most likely to be commonly used after interpolation to standard levels (instead of assimilation model levels) and to an equally-spaced grid in latitude and longitude (2.5 degree interval) instead of each model's grid or spectral coefficients. Since that will be the common usage, the comparisons made here also use such interpolated data. For example, NCEP reanalyses are originally spectral coefficients truncated at T62 in the horizontal and 28 sigma (terrain-following) levels in the vertical. NDRa2 single level fields were provided on a 94 by 192 Gaussian grid that was regridded using NCL to a 73 by 144 equally-spaced (2.5 longitude by 2.5 degrees latitude) grid. This grid at 17 standard isobaric levels is chosen to match the 2.5 by 2.5 degree public domain ERA-40 product. These 17 vertical levels are present in *both* reanalyses: 10, 20, 30, 50, 70, 100, 150, 200, 250, 300, 400, 500, 600, 700, 850, 925, and 1000 hPa. (ERA-40 data at 775 hPa are not used here.) ERA-40 single level fields use the same horizontal resolution. The

ERA-40 public domain web server has much reduced resolution compared to the full ERA-40 data (T159, 60 hybrid sigma levels, see Table 2).

This article has highly restricted purposes. The *first* purpose of this article is to document similarities and differences between two datasets that are likely to be heavily used in the near future. The ECMWF ERA-40 reanalysis will be compared with the NCEP/DOE NDRa2 data. This article will ***not*** attempt to evaluate which dataset is "more correct" such an evaluation is outside the intended scope of this work. However, several studies are cited here that have discussed the relative merits of the NNRa1, ERA-40, and similar datasets though often in certain restricted situations.

Interested readers can find various ERA-40 seasonal and annual average fields depicted in an atlas published by ECMWF (Kållberg et al., 2005). Interested readers can presently create plots of NDRa2 data online at NCEP websites such as: http://www.cdc.noaa.gov/cdc/data.ncep.reanalysis2.html. However, very few fields can be directly compared (e.g. no zonal averages) using the ERA-40 atlas and NDRa2 websites. So, a *second* purpose of this article is to make such comparisons for fundamental general circulation variables.

To compress the presentation, only DJF (December, January, and February average) and JJA (June, July, and August average) results are shown. The months used are all JJA and DJF from January 1979 – December 2000. All fields described are time averages where the two datasets overlap in time using the same variable naming convention. (some NDRa2 variables change name after 2000.) Many variables are also averaged over longitude, such zonal averaging is indicated by using square brackets around the variable name.

Some fields don't have a precise match between datasets (such as radiation and cloud fields) which limits the scope of the comparisons made here. Even so, datasets are used as available on line and as would be relevant to general circulation studies. Instructors preparing course materials, students doing homework, even researchers who

do not have connections with those who prepared the data will limit their attention to what is available on line. So this study has similar limitation. The reduced resolution should not materially alter the comparisons of the large scale features made here.

2. Comparisons

2.1. Radiative fields (TOAswrf, TOAlwrf, sswrf, slwrf)

In studying the general circulation, the radiation fields are of primary importance since the uneven distribution of absorbed solar radiation is the ultimate driving force behind the general circulation. However, the radiation fields in the datasets may not be adequate for studying the general circulation. Trenberth (personal communication) says they are insufficient, since these fields are dominated by clouds which are not simulated well enough by the models used to generate the analyses. Allan et al. (2004) make a much more extensive comparison (than here) between ERA-40, NNRa1, and satellite measurements of various radiative properties.

Further limiting our comparison of radiative fields is the issue that different types of radiation fields are provided in the available datasets. However, downward short wave and long wave radiation at the Earth's surface and top of atmosphere (TOA) are available for comparison in both datasets.

Net downward shortwave radiative flux at the top of the atmosphere (TOAswrf) indicates the solar radiative input into the earth-ocean-atmosphere system. TOAswrf is obviously larger in the summer hemisphere due to the tilt of the Earth's axis. On a global average, TOAswrf is slightly larger in ERA-40 than NDRa2 Global means during DJF: 240.31 in NDRa2 and 243.00 in ERA-40; during JJA: 230.63 in NDRa2 and 231.44 in ERA-40. (The global means were calculated with a NCL-supplied zonal averaging and simple trapezoidal rule with cosine latitude weighting in latitude.) Allan et al. (2004) compare global annual means of absorbed solar radiation from NNRa1 with ERA-40; the NDRa2 values appear to improve upon NNRa1 values and are larger than NNRa1 by

roughly 10 W m^{-2}. Allen et al. (2004) state the global annual mean ERBE value as 238 W m^{-2} which is perhaps closer to the ERA-40 range. [TOAswrf] (Fig. 1) is systematically larger in the summer polar region by > 20 W m^{-2}. (The symbols: [ ] are used in this paper to indicate zonal average.) There is also some tendency for ERA-40 data to be lower in the summer hemisphere middle latitudes, by ~10 W m^{-2}. Close to the equator, the ERA-40 data tend to be larger by 10-25 W m^{-2} depending on the season. Geographically, the primary contributors to the higher equatorial values in ERA-40 are the eastern Pacific and the Atlantic Ocean regions. Some of the difference field in the eastern Pacific is dipolar and consistent with the ICZ (judged from vertical motion, see below) being much narrower and further North there in ERA-40 data. The Atlantic TOAswrf difference also reflects a narrower ICZ in ERA-40 data (and the missing ICZ in NDRa2 during DJF, see precipitation results below). The high latitude summer difference seems linked to snow covered regions; during JJA the larger difference between datasets is over Greenland, with opposite sign to the difference over ice-free Siberia and North America. During DJF the TOAswrf is less (by 20-40 W m^{-2}) over the South Pacific Convergence Zone (SPCZ) which is more strongly defined (e.g. with higher estimated total cloud cover) in ERA-40 data. The equatorial side of the summer subtropical highs has greater TOAswrf in ERA-40 data, again total cloud cover is consistent in being estimated to be less there in ERA-40 data.

Zonal mean net upward longwave radiative flux at the top of the atmosphere, [TOAlwrf] tends to be 2-5% larger in ERA-40 over the winter midlatitudes. See Fig. 2. Near the equator, on the summer side, ERA-40 is less by as much as 15 W m^{-2} though the two datasets agree better right at the equator. For shortwave and longwave radiation near the equator the TOA curves have more prominent ‘dips’ or ‘bumps’ in the ERA-40 data; the primary reason for this difference is the ICZ has narrower meridional extent in ERA-40 data over the Atlantic and the eastern Pacific. Where both datasets have an ICZ, they agree well in zonal mean data, where NDRa2 has a wider ICZ, they have larger disagreement. As with TOAswrf, the longwave flux in the region of the SPCZ is less in ERA-40; a result that would be consistent with estimated greater high cloudiness (not shown) there in ERA-40. Over nearly all of the Southern Hemisphere middle latitudes,

ERA-40 has slightly higher TOAlwrf (and lower TOAswrf). In the tropical, northwestern Pacific and to a lesser extent the Indian ocean ICZ, ERA-40 has much smaller TOAlwrf (and smaller TOAswrf) in both seasons, but especially in summer (JJA), consistent with estimated total cloud cover (not shown) being 10-20% greater there in ERA-40 data. The differences over the Indian and west Pacific ICZ exceed 30 W m^{-2} over a large area; the disagreement exceeds 25%(!) in the South China Sea during JJA and Timor Sea during DJF. Outgoing longwave radiation (OLR) in this region is discussed in detail by Neuman et al. (2000; DJF); comparing ERA15 with NNRa1 and other data, some areas ERA15 performs better, some areas NNRa1 performs better. Speculating about the ERA-40 versus NDRa2 differences seen here, perhaps there are more high clouds or colder cloud tops over the South China Sea and Timor Sea in NDRa2 data. Such excess ERA-40 tropical cloudiness seems consistent with the model creating excessive tropical precipitation during the first 6 hours (Uppala et al., 2005). Allan et al. (2004, their Fig. 13) compare ERA-40 with ISCCP data from 1983-1993 and also find greater cloud cover in tropical 'convective regions' (e.g. western Pacific) by 10% or more. Elsewhere in winter, major ice fields (Antarctica and Greenland) have smaller TOAlwrf in ERA-40 whereas the north Atlantic, Barents Sea, and most of Russia have larger TOAlwrf in ERA-40.

Global averaging of TOAlwrf estimates the heat lost by the planet. Global means during DJF: 240.52 in NDRa2 and 242.71 in ERA-40; during JJA: 245.88 in NDRa2 and 247.62 in ERA-40. These values straddle global *annual* means for ERA-40 and NNRa1 shown by Allan et al. (2004). Allan et al (2004) also give annual observed values from ERBE of 235 W m^{-2} which is less than these reanalysis values, though perhaps closer to NDRa2. The longwave flux leaving the planet should agree with the net short wave flux absorbed by the planet if the planet is not heating or cooling in the net. The downward solar and upward terrestrial values agree to within 0.3 W m^{-2} during DJF. But it puzzles the author that during JJA, *the upward exceeds the downward radiative flux in both datasets by ~15 W m^{-2} at the top of the atmosphere, suggesting net cooling of the planet during JJA.* The scheme used for calculating the global mean is not exact, but would not be expected to have an error as large as 15 W m^{-2}. Allan et al. (2004) find comparable,

annual average net radiative cooling of 7.4 W m^{-2} for ERA-40 and even larger cooling for NNRa1 data, however, the NDRa2 data may have smaller imbalance than the NNRa1. Yang et al. (1999) compare NNRa1 data with ERBE for 1985-6. Allan et al. (2004) felt the TOA radiation budget was better simulated in NNRa1, which they attribute to inaccurate cloud properties. Uppala et al. (2005) also notice "about 7 W m^{-2}" global average cooling when comparing incoming and outgoing radiative flux at the TOA.

Surface solar radiative flux (sswrf) downwards is more similar in the winter hemisphere than in the summer hemisphere, Fig. 3. On a zonal mean, ERA-40 values tend to be lower in the winter middle latitudes (by roughly 5-20 W/m^2). In the higher latitudes during summer, ERA-40 data is generally much less than NDRa2 data. For example, differences between datasets range from 30 W/m^2 at 40N to 100 W/m^2 (!) at the North Pole during JJA. ERA-40 [sswrf] is similarly lower over much of Antarctica and adjacent ocean during DJF, except near the South Pole. The ICZ (intertropical convergence zone) is more narrowly defined (by a minimum in [sswrf]) which is also a little north of the corresponding minimum in NDRa2 data. Geographically, stronger differences occur over the Sahara and Arabian deserts, with ERA-40 being larger by >20 W/m^2 over much of those deserts. Over the high elevations of Tibet, Rockies, and Andes, NDRa2 is larger by typically 40-80 W/m^2 with isolated points exceeding 150 W/m^2 difference, with the larger differences occurring in summer. Also in summer, NDRa2 data is larger over the subtropical oceans. The differences in handling the ICZ are most apparent over the tropical oceans. ERA-40 is larger by >40 W/m^2 in the Eastern Pacific (DJF and JJA) and across the Atlantic (mainly JJA). Some of the difference follows from NDRa2 having a latitudinally broader area of cloudiness in the Atlantic ICZ in JJA (also for the east Pacific ICZ in DJF). In the Indian Ocean the reanalyses are more similar though NDRa2 is larger along much of the ICZ. The global mean values of sswrf in DJF are 190.88 for NDRa2 and 185.08 for ERA-40; and in JJA the global means are 179.88 and 169.14, respectively.

Surface thermal radiative flux (slwrf) downwards is quite similar in both datasets; see Fig. 4. On a zonal mean, ERA-40 [slwrf] values tend to be larger (by 5-10 W/m^2)

than NDRa2 values in middle latitudes. NDRa2 tends to have higher [slwrf] values for the subtropical region of sinking motion associated with the winter Hadley cell; a result of higher values over the oceanic regions, which are very uniformly higher (by >10 W/m^2) in NDRa2 data. ERA-40 [slwrf] values are considerably higher in the summer polar regions (12-16 W/m^2 during DJF over Antarctica; 20-45 W/m^2 over the Arctic in JJA). Geographically, the largest differences are found over mountainous regions, in particular: the Andes, Rockies, and Himalayas where ERA-40 is larger (>90 W/m^2 at some grid points!). Generally, ERA-40 has larger values (~20 W/m^2) over much of the Sahara. The global mean values of slwrf in DJF are 332.64 for NDRa2 and 335.50 for ERA-40; and in JJA the global means are 348.57 and 352.66, respectively.

Notable differences between ERA-40 and NDRa2 radiation fields discussed here are summarized in Table 3.

2.2. Temperature (T)

Zonal mean temperature in the middle to lower troposphere, between 30S and 90N, is similar in both reanalyses; [T] differences seen in Fig. 5 are generally less than 1 K. Near the tropical tropopause, [T] in ERA-40 is ~3 K colder than NDRa2. (The peak difference occurs near 100 hPa and is spread over 20-40 degrees of latitude.) In the stratosphere above (20-50 hPa) NDRa2 is colder by ~1 K. In Southern Hemisphere midlatitudes, [T] is colder in ERA-40 by ~1 K, especially in the lower and upper troposphere in both seasons. Over Antarctica, [T] below 500 hPa is warmer in ERA-40 (up to 3.5 K, though the highest values are bogus, being for pressure levels that are "underground"), while in the upper troposphere (150-400 hPa) ERA-40 is colder (up to 3.5 K) than NDRa2. The difference is roughly twice as large during summer and has a clear impact upon sea level pressure, as might be expected. In the ocean areas adjacent to Antarctica, lower tropospheric [T] is warmer by a degree or so in NDRa2. Geographically, the difference in T at 150 hPa is greatest above the southern subtropical oceans all year, the northern subtropical oceans in JJA, and over Antarctica in JJA. In the tropics, T at 150 hPa has largest difference in the eastern Pacific and across the Atlantic during JJA (warmer in

NDRa2, see Fig. 5). Near the Earth's surface, T at 925 is about a degree warmer in NDRa2 over nearly all the oceans, somewhat consistent with slwrf results shown above. Exceptions are eastern subtropical ocean areas (near: Mexico, Peru, Angola) of persistent low stratus during JJA. Over much of Africa, ERA-40 is warmer, by 2 to 4 K over most of the Sahara (DJF and JJA) and southern Africa (especially winter, by >2K). Generally, areas with higher elevation (*n.b*. some of these have surface pressure less than 925 hPa) are warmer in ERA-40. Some notable differences between ERA-40 and NDRa2 temperature fields are summarized in Table 4.

Trenberth et al. (2001, their Fig. 5) compare ERA15 and NNRa1 zonal mean temperatures and find ECMWF data to be cooler than NCEP data by more than 2 K near the tropical tropopause; that difference is reported as robust during sub-periods and appears quite similar to the difference reported here with ERA-40 and NDRa2 data. They also find ERA15 data cooler (by 1 K) in the lower troposphere of the Southern Hemisphere midlatitudes, again this difference continues with the longer, more recent data compared here. Randel et al. (2004) compare ERA-40 with other datasets covering the stratosphere; they state that the ERA-40 zonal mean values at 100 hPa and between 5S to 5N are close to the average of 8 nearby radiosondes while NNRa1 data are systematically several degrees warmer. Simmons et al. (2004) remark that the ERA-40 data in the time period studied here has a mid tropospheric 'cold bias' by roughly a degree in the Southern Hemisphere middle latitudes. Bromwich and Fogt (2004) compare two meter T in ERA-40 and NNRa1 interpolated to Antarctic stations and find better correlations, bias, and root mean square error (rmse) in the ERA-40 data.

2.3. Mass fields (slp, Z)

Sea level pressure (slp, not shown) has similar zonal mean in the two models north of 65S. Zonal mean differences are generally less than 1 hPa except in polar regions. North of 55N during DJF, [slp] differences approach 2 hPa at the North Pole. South of 65S, [slp] is much lower (by up to 12 hPa) in ERA-40. The [slp] differences are greater during summer, as was [T]. [slp] over topography is extrapolated from surface

pressure using an exponential. The exponential argument is inversely related to surface temperature so the extrapolation from surface pressure is greater in NDRa2 (since it is colder) than in ERA-40, consequently, NDRa2 has higher [slp]. Geographically, the only noteworthy differences are associated with topographic features. ERA-40 slp is much less (>20 hPa in JJA, half that in DJF) over much of Antarctica, and less over the Tibetan plateau especially during the local winter (>6 hPa in DJF, half that in JJA). The global mean slp during DJF is 1011.43 hPa in NDRa2 and 1011.45 hPa in ERA-40; during JJA the corresponding means are 1011.45 and 1011.20. Trenberth and Smith (2005) have compared a different quantity, *surface* pressure, and found larger differences between NNRa1, ERA-40, and ERA-15 than found for global mean *sea level* pressure here; they find global mean surface pressure was ~0.3 hPa greater in ERA-40, than NNRa1. Unfortunately, surface pressure is not in the online ERA-40 products supplied by the ECMWF public domain server. Bromwich and Fogt (2004) compare ERA-40 and NNRa1 data interpolated to stations in the Southern Hemisphere middle and polar latitudes. During the satellite era they find consistently better performance (correlation, bias, rmse) in ERA-40. They further remark that NDRa2 data is "very similar" over the period of overlap with NNRa1. Both ERA-40 and NNRa1 did worst during local winter.

Geopotential height (Z, not shown) responds predictably to the T differences in the datasets. [Z] throughout the middle and lower troposphere (>400 hPa) north of 50S has less than 10m difference between the datasets. In the tropical lower stratosphere, ERA-40 [Z] heights are lower (by ~90 m in DJF, by ~50 m in JJA); this difference reflects the lower tropical tropopause temperatures mentioned above. Geographically, the largest differences in Z at 150 hPa are above: Antarctica, the Southern Hemisphere oceans, and the northern oceans (mainly JJA). The smallest differences (<20 m) tend to occur over Australia, and landmasses north of 20N. Over Antarctica, the colder temperatures of the NDRa2 reanalysis lead to lower heights; the difference in [Z] is about 20 m at levels between 300 and 500 hPa over Antarctica. Bromwich and Fogt (2004) compare 500 hPa heights in ERA-40 and NNRa1 interpolated to Southern Hemisphere polar and middle latitude stations. ERA-40 was generally superior in correlation, bias,

and rmse over Antarctica. Some notable differences between ERA-40 and NDRa2 mass fields are summarized in Table 5.

2.4. Velocity fields (U, V, ω, meridional circulation)

Zonal mean zonal wind [U] is similar in both analyses through much of the troposphere as might be anticipated from the similar [Z] fields (geostrophic wind considerations). The Southern Hemisphere subtropical jet is stronger in ERA-40 by 1-2 m/s. See Fig. 6. However, an intriguing difference is found in the tropical upper troposphere during DJF. The difference in [U] between 100 to 200 hPa and 10S to 5N is about 2 m/s. This seemingly small difference is sufficient to reverse the sign of [U] in that region; weak westerlies occur in ERA-40 and weak easterlies occur in NDRa2. During JJA, both datsets have tropical easterlies through the depth of the troposphere, though the westerlies extend deeper into the tropics in the Southern Hemisphere levels near the tropopause in ERA-40. In the lower stratospheric subtropics, ERA-40 data has stronger [U] easterlies (by several m/s) than the NDRa2 reanalysis.

Geographically, during DJF both datasets have westerlies at 150 hPa over the eastern Pacific and central Atlantic; in ERA-40 these westerlies are 4-9 m/s more westerly. (See upper panel, Fig. 7) The region of westerlies is similar in the east Pacific but is broader (longitudinally) in the Atlantic (near 20S). Dynamical theory (Webster and Holton, 1982; Branstator, 1983) suggests that tropical easterlies will reflect energy approaching the equator whereas westerlies would allow such information (apparent as a stationary wavetrain) to propagate into the opposite hemisphere. Theory predicts that the stronger the westerlies, the easier the interhemispheric propagation, so the datasets appear to allow different interhemispheric communication. Easterlies in ERA-40 are also several m/s slower over the equatorial Indian Ocean during DJF.

During JJA, equatorial easterlies are stronger by several m/s in ERA-40 over the eastern Pacific and western Atlantic (e.g. 150 hPa level; lower panel, Fig. 7). One consequence is the longitudinal range of tropical westerlies over northern South America

is stronger and wider in NDRa2 (>2 m/s from 60 to 70W) than in ERA-40 somewhat contrary to the DJF result.

Meridional motions on the zonal mean, [V, not shown] emphasize the winter hemisphere Hadley circulation. The upper tropospheric "return flow" of the winter hemisphere Hadley cell in ERA-40 has stronger peak value (3.5 m/s in NDRa2 versus 4 m/s in ERA-40) and extends through a greater depth (higher and lower) during DJF. During JJA, the ERA-40 return flow is again stronger (by ~0.5 m/s) and a bit deeper. Geographically, the JJA return flow has larger differences between datasets along a band extending across the equatorial Indian ocean to the eastern Pacific; V is stronger, by >1.5 m/s, in NDRa2 data. However, the return flow over the subtropical Atlantic and southern Africa is a bit weaker in NDRa2 JJA data. In DJF, the prime contributors to the stronger ERA-40 return flow are over the Sahara, and along a band from the northeastern Indian Ocean across most of the equatorial Pacific.

Zonal mean pressure velocity [ω] has a single large maximum in NDRa2 DJF data but two distinct maxima in ERA-40 DJF data (Fig. 8). That second maximum causes [ω] in ERA-40 to differ from NDRa2 by about half the magnitude of the primary maximum. The secondary maximum found only in ERA-40 DJF [ω] is centered near 5N. Geographically, the source of the secondary maximum is the ICZ over the eastern Pacific and central Atlantic; the ICZ in those regions is much stronger and meridionally narrower in ERA-40 data (Fig. 9). In fact, NDRa2 ω data has *sinking* where one might expect rising for an Atlantic ICZ during DJF. Over the Indian Ocean and consistent with [V] data, the rising motion is broader and more zonally-varying in NDRa2 data. During JJA, the NDRa2 data recover an Atlantic ICZ, though it is broader and weaker than in ERA-40. Even though the grid points are the same, the NDRa2 ω field is noticeably smoother than the same field in ERA-40 data. JJA ERA-40 data have a 'wavier' ω field near major steep-sloped topographic features such as the Andes, Rockies, and Himalayas.

The changes to vertical and meridional motions show up in somewhat coherent difference fields of the zonal mean meridional circulation. Fig. 10 shows arrows

depicting the mean meridional cells. The winter Hadley circulation is the most prominent feature. Also shown is the 'difference circulation' constructed from the difference between ERA-40 and NDRa2 fields of [V] and [ω]. The DJF difference circulation has some indication of the missing or weaker Atlantic and eastern Pacific winter Hadley cell circulations in NDRa2 data. In JJA data the difference circulation again shows some evidence for a weaker winter Hadley cell in NDRa2 data. Close inspection finds that some low level arrows of the difference circulation oppose each other, most notably in the DJF panel; a result that reflects the stronger ICZ in ERA-40 in the eastern Pacific, a portion of the ICZ that has less seasonal migration than elsewhere along the ICZ. Some differences between ERA-40 and NDRa2 velocity fields are summarized in Table 6.

2.5. Moisture (q, total cloud cover, P)

Specific humidity (q) is provided in the ERA-40 data but must be created from T and relative humidity at isobaric levels in the NDRa2 data. Specific humidity (Fig. 11) is largest in the tropical lowest levels, decreasing rapidly towards the poles and with increasing elevation. The zonal average, [q] has greatest magnitude difference between the datasets in the tropical lower half of the troposphere. Generally, [q] is much larger (ranging from 5-25%) in ERA-40 data in much of the mid to lower troposphere of the tropics. Andersson et al. (2004) note that the assimilation scheme for satellite data increased tropical moisture. In the lower half of the troposphere in the adjacent subtropics, [q] is less (by 5-20%) in ERA-40. The difference (ERA-40 minus NDRa2) is positive from 20S to 10N during DJF and from equator to 30N during JJA for pressure greater than 300 hPa. Trenberth et al. (2001) also find higher specific humidity values in ERA-40 data in the lower half of the tropical troposphere compared with NNRa1.

The geographic distribution of the difference at representative 700 (shown) and 850 (not shown) hPa levels are as follows. During DJF, ERA-40 has greater q in the Atlantic ICZ across equatorial Africa; ERA-40 is ~15% larger along the ICZ across the southern Indian ocean into the western Pacific; ERA-40 is also wetter (by ~15%) in the south Pacific convergence zone (SPCZ). In the eastern Pacific, south of the equator,

ERA-40 is generally drier by up to 20% at 700 hPa (but not so at 850 hPa). During JJA, the differences at 700 and 850 hPa are as follows. The difference is positive over most of the northern tropical oceans, especially along the ICZ across the Pacific, Atlantic, Africa, and northern lowland India; ERA-40 is up to a third larger than NDRa2. Also, much of the tropical Indian Ocean and New Guinea are more than 1 gm/kg moister in ERA-40 at 700 and 850 hPa. The SPCZ is narrower in ERA-40 leading to larger negative differences during JJA in the South Pacific. NDRa2 has more water vapor over much of the northern side of the south Pacific subtropical high and that is consistent with the wider SPCZ mentioned. In the south Indian Ocean, a dipolar difference at 700 hPa results from topical NDRa2 having less peak moisture (at the equator) but extending further south before having a sharp meridional gradient.

The total cloud cover is expressed as a percent fraction of the sky. Total cloud cover is provided in ERA-40 whereas the NDRa2 data have total cloud cover at various levels or ranges of levels. Hence it is not possible to directly compare the datasets. One cannot determine either variable from the other without making assumptions. As a rough comparison, it is assumed that the total cloud cover equals the fraction of high cloud cover plus the fraction of clear sky at high level multiplying the fraction of cloud cover at middle level, plus the remaining fraction of clear sky multiplying the fraction of lower level cloud. When estimated this way, the NDRa2 data are similar in range to the ERA-40 data: matching well for the ICZ maximum and summer subtropical minimum, ERA-40 being cloudier in the winter subtropics and year around in polar regions. Again, these comparisons are not precise.

Frequent mention has been made here of ERA-40 data having narrower ICZ in the Atlantic and eastern Pacific. Cloud climatologies from satellite data (e.g. Miller and Feddes, 1971; see also Grotjahn, 1993, plate 2 and fig. 5.13) show quite a narrow time mean ICZ-related cloudband across the eastern Pacific and a less narrow cloud band across the Atlantic. Such cloud climatologies seem more comparable to the ERA-40 depiction. A comparison of ERA-40 and ISCCP decadal time mean (Allan et al., 2004)

shows agreement to within 10% over the Atlantic and eastern Pacific, with ERA-40 being roughly 10% too cloudy in the western Pacific.

Precipitation rate (P) is presented here as mm per day and has largest maximum along the tropical ICZ. See Fig. 12. (Note: the data on the ECMWF public domain server is based on 0 to 6 hour forecasts of P. Uppala et al. (2005, p. 2997) state that P data at longer forecast periods (12-24 hr) agree better with GPCP values.) Secondary maxima occur in middle latitudes associated with frontal cyclone storm tracks. During DJF, [P] has a double maximum in the tropics in ERA-40 data but a single maximum in NDRa2 data; this result is consistent with the vertical motion field in Fig. 8. Geographically, the DJF difference shows that ERA-40 has much larger P (often by 50 - 100%) along the Atlantic and eastern Pacific ICZ, again as might be anticipated from greater upward motion there in the ERA-40 data. The subtropical minimum is a bit lower in ERA-40 in both hemispheres and both seasons. The middle latitude secondary maximum is generally larger for NDRa2 data for the Northern Hemisphere during both DJF and JJA. In the Southern Hemisphere during JJA the midlatitude maximum is about the same during DJF, but during JJA NDRa2 [P] is again larger. Geographically, JJA precipitation rate along the eastern Pacific ICZ is again stronger in ERA-40 data over the oceans. In contrast to DJF, precipitation rate along the Atlantic ICZ is stronger in NDRa2 data. NDRa2 is also locally much larger (by up to 100% more) over southern India and southeast Asia. As Neuman et al. (2000) noticed for the precursor datasets ERA15 and NNRa1, both ERA-40 and NDRa2 have a ‘double’ ICZ across the western half of the Pacific (from roughly 160W to 120E) in DJF. In JJA ERA-40 has a double ICZ of similar extent, but NDRa2 does not owing to a stronger northern branch of ICZ in the west Pacific ‘warm pool’. Also, while the island of New Guinea has more P in ERA-40, the Pacific Ocean to the north has less P in ERA-40 than NDRa2. The greater New Guinea P may reflect different topographic formulations in the models used by the two datasets. ERA-40 is also larger in narrow regions of the west coast of Central America and Columbia. In the Northern Hemisphere midlatitudes, NDRa2 data are larger over the oceanic storm tracks during DJF; but during JJA, NDRa2 data are larger mainly over land areas, specifically: northwestern Canada, southeastern United States, eastern Europe, and

northwestern Russia. The global average P in DJF is 3.03 in NDRa2 and 3.12 in ERA-40; in JJA the global means are 3.28 and 3.12, respectively.

Andersson et al. (2005) discuss the hydrological cycle in ERA-40 stating (p. 390) that "excessive tropical oceanic precipitation is arguably the most serious problem diagnosed in ERA-40." One reason to question the ERA-40 P is that the ERA-40 data are not in hydrological balance (Andersson et al., 2005, and references therein). Andersson et al. further show that ERA-15 data during the period: 1989-93, had better water balance, and NNRa1 in the early satellite period (1973-1975) had better water balance than ERA-40 during those periods. The geographical pattern of relative wetter and dryer regions is apparently satisfactory (Betts and Beljaars, 2003) but the global average has unrealistic excess P over evaporation (Hagemann et al., 2005). Other studies have compared P in the precursor datasets. In the Arctic, Serreze and Hurst (2000) are critical of NNRa1 P data while concluding that ERA15 data are superior. In the Asian monsoon region Annamalai et al. (1999) compare NNRa1 and (essentially) ERA15 data over the 1979-1995 period. They conclude that the ECMWF data is superior. Comparing the same time period (not shown) some aspects of P in NDRa2 have improved noticeably over NNRa1, though other aspects may be less well. NDRa2 matches observational datasets of Legates and Willmott (1990) and Xie and Arkin (1996) better than did NNRa1 at the SW coast of India and the Myanmar coast; previously NNRa1 P was much too weak, now NDRa2 P may be a bit too strong. (ERA-40 data are much smaller at both places.) In the western Pacific those observational datasets seem better matched in some regions (north of New Guinea) by NDRa2 than ERA-40 during that time period; in other areas ERA-40 looks comparable or qualitatively better. Over the Himalayas, NDRa2 has less P than NNRa1 becoming perhaps too little compared to those observational datasets, while ERA-40 is much larger than the observational datasets.

Some notable differences between ERA-40 and NDRa2 moisture-related fields are summarized in Table 7.

2.6. Energetics (SHF, LHF, MSE, KE)

Surface sensible heat flux (SHF, Fig. 13) is available in both datasets. Surface sensible heat flux plays a role in exchange of energy between the atmosphere and the earth's surface. In both datasets, SHF is positive over oceans in the tropics and most of the middle latitudes of the winter hemisphere. Near the western boundary currents in winter, SHF is large in both datasets, but is 20-50% larger in NDRa2. Over North America and Eurasia in DJF, SHF is negative and more strongly so in NDRa2 data. In contrast, during JJA, the Northern Hemisphere continents have positive SHF which is more similar in the two datasets. ERA-40 tends to have larger positive SHF over the oceans (except Arctic) in JJA, too. SHF is negative over most of the Arctic, and perhaps more strongly so in NDRa2 data. These geographic variations cause [SHF] to be systematically larger in ERA-40 data. The difference in [SHF] between datasets tends to increase towards higher latitudes, exceeding 10 W/m^2 in polar regions. The global mean of SHF in DJF is 6.06 in NDRa2 and 14.00 in ERA-40; in JJA the global means are 10.05 and 16.99, respectively.

Another component of the surface energy budget is surface latent heat flux (LHF, Fig. 13). Unlike [SHF], [LHF] is positive for all latitudes in both datasets. [LHF] is also often much larger than [SHF]. Both datasets have relative maxima of [LHF] in the subtropics. The two maxima are similar in DJF; in JJA the Southern Hemisphere max is about 20% larger. The fluxes generally decrease towards the poles, with a weak secondary maximum at high northern latitudes. The [LHF] is systematically less in ERA-40 data for most latitudes north of 30S. Differences in [LHF] range around 5-20 W/m^2 at many latitudes. Recall that the corresponding [SHF] difference had opposite sign in these latitudes. The two datasets have quite similar [LHF] in latitudes south of 30S. The global mean of LHF in DJF is 88.86 in NDRa2 and 81.55 in ERA-40; in JJA the global means are 93.27 and 84.91, respectively. Geographically, NDRa2 data is larger than ERA-40 data over nearly all of the tropics, both ocean and continental areas. The difference is largest where the field is larger, such as the non-ICZ portion of the tropical Atlantic (during JJA: 5N to 20N and 10S to 15S where differences exceed 40 $W\ m^{-2}$).

For tropical and some subtropical latitudes moist static energy (MSE) decreases with increasing elevation in the lowest 200-300 hPa due to the rapid decline of specific humidity as elevation increases. Elsewhere in the troposphere, MSE increases with elevation due to the statically stable nature of the atmosphere. MSE increases even more rapidly with increasing elevation in the stratosphere due to high static stability. MSE change with elevation is crucial for a mass-conserving circulation like the Hadley cell to have a net transport of heat. To transport heat poleward, the upper branch of the Hadley cell must be in air of higher MSE than the equatorward flow underneath. In the tropics and low subtropics, this net vertical difference in heat transport is much smaller (by a couple orders of magnitude) than each of the opposing heat transports. Hence, even though the difference in MSE between ERA-40 and NDRa2 is about 1% of the magnitude of MSE, the impact of the MSE difference upon the meridional transport of heat may be substantial. The larger differences (excluding areas of high topography) are primarily near the oceanic ICZ. It is shown above that the ERA-40 data have higher q (specific humidity) in the lower troposphere and lower temperature in the upper troposphere; this combination means that the difference in MSE between upper and lower troposphere is less in the ERA-40 data than in NDRa2 data. It is also shown above that the ERA-40 data have a stronger Hadley circulation. Hence, compared to the NDRa2 heat transport, ERA-40 data have a faster circulation that could be compensating for a smaller vertical difference in MSE. These properties of [MSE] are seen in Fig. 14.

Calculation of the net meridional heat flux is a vertical integral that is not easily made precise from the supplied data. The vertical integral from 1000 to 10 hPa of [V] should be nearly zero, except for interhemispheric mass transfers. Using a crude trapezoidal rule approximation to that integral yields vertical mean [V] at 5N during DJF of: 3 mm/s in NDRa2 and 41 mm/s in ERA-40; the corresponding values at the equator in JJA are: -21 mm/s in NDRa2 and -64 mm/s in ERA-40. These estimates are too crude to trust fully when calculating corresponding net heat fluxes. With that caveat, the corresponding net heat fluxes are similarly different: ERA-40 values of the net heat flux tend to exceed the NDRa2 values when calculated this way. For the indicated latitudes and seasons, the net heat flux is 6-12 times larger in ERA-40. The tropical tropopause is

near the data level 100 hPa. If the integration range in pressure is restricted to 100 to 1000 hPa, the net vertically integrated meridional velocity and MSE flux are even worse, with DJF NDRa2 values having incorrect sign for MSE flux. Clearly these results are discouraging and use of either dataset to deduce net heat fluxes requires caution and more care. The interested reader is directed to Trenberth et al. (2002) for a much more thorough discussion of how to properly calculate vertical integrals from data interpolated to isobaric levels.

Kinetic energy (KE, Fig. 15) is larger in ERA-40 data than in NDRa2 data. As noted above, the [U] subtropical jet stream is stronger in ERA-40 data, especially in the Southern Hemisphere during winter. In the Northern Hemisphere the difference is larger again during winter. The stratospheric polar night (winter) jet is stronger and wider in ERA-40 data during DJF making the winter polar stratospheric KE about 1/3 larger and extending further poleward; in JJA, the [KE] magnitudes are similar between datasets, but the ERA-40 data again extends further poleward, leading to large differences. Finally, the datasets differ in the stratospheric equatorial [KE], which is more than twice as large in ERA-40 data. Geographically, the differences mirror differences seen in zonal wind. At 200 hPa and during DJF, ERA-40 has higher KE over the southern ocean subtropical jet (>100 $m^2 s^{-2}$), the southeastern tropical Pacific (>140 $m^2 s^{-2}$), northern hemisphere subtropical jet (> 140 $m^2 s^{-2}$) over the western Pacific with peak differences closer to 120 $m^2 s^{-2}$ over Asia and northern Africa. At 200 hPa and during JJA, ERA-40 data are again stronger over the subtropical jets of the south Pacific (> 175 $m^2 s^{-2}$) and south Indian (>250 $m^2 s^{-2}$) Oceans, the Northern Hemisphere jet is stronger (>100 $m^2 s^{-2}$) only east of Japan. As noted above, NDRa2 has a stronger JJA tropical Indian ocean easterly jet, so NDRa2 KE is larger (>100 $m^2 s^{-2}$) there. It is speculative, but extratropical KE being larger in ERA-40 than NDRa2 may be related to how satellite data is input. Bengtsson et al. (2004) find hemispheric average KE increases (DJF KE is 11% larger in the Southern Hemisphere extratropics) when satellite data are included in the ERA-40 assimilation versus using no satellite data. Table 8 lists some noteworthy differences between ERA-40 and NDRa2 energy-related fields.

3. Conclusions

In recent years a huge effort has been made at operational centers in the U.S. and ECMWF to make available internally consistent, long term, stable collections of gridded atmospheric data. Two important, recent datasets, here labeled NDRa2 and ERA-40 have been compared. The resolution of the NDRa2 data have been reduced to the ERA-40 public data resolution of 2.5 by 2.5 degrees longitude and latitude with 17 isobaric levels. The ERA-40 public data is greatly reduced from the archived ERA-40 data. It is beyond the scope of this article to assess which dataset is "more correct" and the author is loath to do so given the great value of each dataset and the great effort expended to produce and make easily available both datasets. Earlier 'precursor' versions of the datasets have been compared by others, though for a more limited region or set of variables. For example, Bromwich and Wang (2005) compare ERA15, ERA-40, and NNRa1 data over the Arctic against selected radiosonde stations and conclude that ERA-40 capture better properties seen in the observations.

The datasets disagree in some global mean radiative properties, but those who study radiation probably would seek out other sources, such as working with satellite data directly. Many of the differences quantified here agree qualitatively with comparisons of the precursor datasets (ERA15 and NNRa1) made by others and those are noted above.

Zonal mean differences are often associated with colder tropical upper troposphere temperatures in ERA-40. The zonal mean zonal winds tend to be stronger (especially the jets) in ERA-40 data which also boosts the kinetic energy. The winter Hadley cell is stronger and has more complexity in ERA-40 data.

The solar and infrared radiation have similar values in the tropical regions; where they differ is mainly showing a tendency for the rising in the ICZ to be narrower focused and stronger in ERA-40 data. However, at the surface ERA-40 has more heat entering the atmosphere in sensible form, whereas NDRa2 data have more entering as latent heat. Consequently, specific humidity, q tends to be larger in the subtropics of NDRa2 data.

But since the vertical motion is stronger and maybe more narrowly focused in latitude, ERA-40 has higher q values carried into the middle troposphere close to the equator, with NDRa2 data larger further away, in the subtropics. In the end, the horizontal tropical rainfall is quite similar, except for ERA-40 greater precipitation contributed in the tropical Atlantic and eastern Pacific.

The datasets have some geographic regions where they disagree in many different variables. One of the most significant regions of difference is the treatment of the equatorial regions of the Atlantic and eastern Pacific; in those regions the ICZ is more sharply defined and its vertical circulation appears stronger in ERA-40 data. Topography seems to create other locally large differences, especially the Tibetan Plateau, the Andes, Greenland, and nearly all of Antarctica. Differences in regions of high topography have not been emphasized here because the interpolation to lower resolution grid may be magnifying the differences seen in some regions.

To answer the question posed by the title of this article, the different datasets do give notably different general circulations. In the tropics, the difference is not easily summarized as one dataset having a stronger Hadley cell than the other, since ERA-40 is stronger in some regions (Atlantic and east Pacific) while NDRa2 is stronger in others (Indian and west Pacific). The models differ in their dynamics, with stronger (subtropical and polar night) jetstream winds in the ERA-40 data. ERA-40 has equatorial upper tropospheric westerlies where easterlies prevail in NDRa2 and that may allow more communication between hemispheres in ERA-40's general circulation.

Acknowledgments

ECMWF ERA-40 (ERA-40) data used in this study have been obtained from the ECMWF public data server. The NCEP/DOE AMIP-II Reanalysis (NDRa2) data used in this study have been obtained from the *NOAA/OAR/ESRL PSD, Boulder, Colorado, USA, from their Web site at http://www.cdc.noaa.gov/*. The author greatly appreciates related email correspondence from Drs. Sakari Uppala, Wesley Ebisuzaki, Grant Branstator, Kevin Trenberth, and Masao Kanamitsu. This material is based upon work supported by the National Science Foundation under Grant No. ATM- 0354545.

References:

Allan, R. P., Ringer, M.A., Pamment, J.A., Slingo, A., 2004. Simulation of the Earth's radiation budget by the European Centre for Medium-Range Weather Forecasts 40-year reanalysis (ERA-40), J. Geophys. Res., 109, D18107, doi:10.1029/2004JD004816.

AMIP Project Office, 1996: AMIP II Guidelines. *AMIP Newsletter,* No. 8. [Available online at http://wwwpcmdi.llnl.gov/amip/NEWS/amipnl8.html.]

Annamalai, H., Slingo, J.M., Sperber, K.R., Hodges, K., 1999. The Mean Evolution and Variability of the Asian Summer Monsoon: Comparison of ECMWF and NCEP–NCAR Reanalyses. *Mon. Wea. Rev*. **127**, 1157–1186.

Beljaars, A., Viterbo, P., 1998. The role of the boundary layer in a numerical weather prediction model. Pp. 287-304 in *Clear and Cloud Boundary Layers*. Eds. A. Holtslag and P. Duynkerke. Royal Netherlands Acadmey of Arts and Sciences, Amsterdam, the Netherlands.

Bengtsson, L., Hagemann, S., Hodges, K., 2004. Can climate trends be calculated from reanalysis data? J. Geophys. Res., 109, D11111, doi: 10.1029/2004JD004536.

Betts, A. K. and Beljaars, A. C. M. 2003 'ECMWF ISLSCP-II near-surface dataset from ERA-40'. ECMWF ERA-40 Project Report Series, No. 8. European Centre for Medium-Range Weather Forecasts, Shinfield, Reading, UK (available from http://www.ecmwf.int/publications/library/do/references/lis/)

Branstator, G., 1983, Horizontal energy propagation in a barotropic atmosphere with meridional and zonal structure. J. Atmos. Sci., 40, 1689-1708.

Bromwich, D.H., Fogt, R. L., 2004. Strong trends in the skill of the ERA-40 and NCEP-NCAR reanalyses in the high and midlatitudes of the Southern Hemisphere, 1958-2001. *J. Climate*. **17**, 4603-4619.

Bromwich, D.H., Wang, S-H., 2005. Evaluation of the NCEP–NCAR and ECMWF 15- and 40-Yr Reanalyses Using Rawinsonde Data from Two Independent Arctic Field Experiments. *Mon. Wea. Rev*. **133**, 3562–3578.

Chou, M.-D., 1992: A solar radiation model for use in climate studies. *J. Atmos. Sci.,* **49,** 762–772.

Chou, M.-D., Lee, K.-T., 1996: Parameterizations for the absorption of solar radiation by water vapor and ozone. *J. Atmos. Sci.,* **53,** 1203–1208.

Fels, S. B., and M. D. Schwarztkopf, 1975: The simplified exchange approximation: A new method for radiative transfer calculations. *J. Atmos. Sci.,* **32,** 1475–1488.

Gregory, D., Morcrette, J.-J., Jakob, C., Beljaars, A. C. M. Stockdale, T. 2000. Revision of convection, radiation and cloud schemes in the ECMWF Integrated Forecasting System. *Q. J. R. Meteorol. Soc.*, **126,** 1685–1710.

Grell, G., 1993. Prognostic evaluation of assumptions used by cumulus parameterizations. *Mon. Wea. Rev*., **121**, 764-787.

Grotjahn, R., 1993. *Global Atmospheric Circulations: Observations and Theories*. Oxford Univ. Press., New York, 430 pp.

Hagemann, S., Arpe, K. and Bengtsson, L. 2005 'Validation of the hydrological cycle of ERA40'. In ECMWF ERA-40 Project Report Series, No. 24. European Centre for Medium-Range Weather Forecasts, Shinfield, Reading, UK (available from http://www.ecmwf.int/publications/library/do/references/lis/)

Hernandez, A., Kelly, G. A., Uppala, S. M. 2004. *The TOVS/ATOVS observing system in ERA-40*. ECMWF ERA-40 Project Report Series, No. 16. European Centre for Medium-Range Weather Forecasts, Shinfield, Reading, UK (available from http://www.ecmwf.int/publications/library/do/references/lis/)

Hodges, K., Hoskins, B., Boyle, J., Thorncroft, C., 2003. A comparison of recent reanalysis datasets using objective feature tracking: Storm tracks and tropical easterly waves. *Mon. Wea. Rev.*, **131**, 2012-2037. Corrigendum: 2004. *Mon. Wea. Rev.*, **132**, 1325-1327.

Hong, S. Y., and H. L. Pan, 1996: Nonlocal boundary layer vertical diffusion in a medium-range forecast model. *Mon. Wea. Rev.,* **124,** 2322–2339.

Hortal, M., Simmons, A. J. 1991. Use of reduced Gaussian grids in spectral models. *Mon. Wea. Rev.*, **119,** 1057–1074.

Houghton, J. T., Meira Filho, L. G., Callander, B. A., Harris, N., Kattenberg, A., Maskell, K. (Eds.), 1996. 'Climate change 1995'. In *The science of climate change*. Cambridge University Press, Cambridge, UK.

Kållberg, P., Berrisford, P., Hoskins, B., Simmons, A., Uppala, S., Lamy-Thépaut, S., Hine, R., 2005. *ERA-40 Atlas*. ERA-40 Project Report Series No. 19, 191pp.

Kalnay, E. Kanamitsu, M. Kistler, R. Collins, W. Deaven, D. Gandin, L. Iredell, M. Saha, S. White, G. Woollen, J. Zhu, Y. Leetmaa, A. Reynolds, B. Chelliah, M. Ebisuzaki, W. Higgins, W. Janowiak, J. Mo, K.C. Ropelewski, C. Wang, J. Jenne, R., Joseph, D., 1996. The NCEP/NCAR 40-Year Reanalysis Project. *Bul. Amer. Meteor. Soc*. **77**, 437–471.

Kanamitsu, M., Ebisuzaki, W., Woollen, J., Yang, S-K., Hnilo, J., Fiorino, M., Potter, G., 2002. NCEP–DOE AMIP-II Reanalysis (R-2). *Bul. Amer. Meteor. Soc*. **83**, 1631–1643.

Kistler, R., Kalnay, E., Collins, W., Saha, S., White, G., Woollen, J., Chelliah, M., Ebisuzaki, W., Kanamitsu, M., Kousky, V., van den Dool, H., Jenne, R., Fiorino, M., 2001, The NCEP–NCAR 50–Year Reanalysis: Monthly Means CD–ROM and Documentation. *Bul. Amer. Meteor. Soc.*, **82**, 247–267.

Legates, D. R., Willmott, C.J., 1990: Mean, seasonal and spatial variability in gauge corrected global precipitation. *Int. J. Climatol.,* **10,** 111–127.

Mahrt, L., and K. L. Pan, 1984: A two layer model of soil hydrology. *Bound.-Layer Meteor.,* **29,** 1–20.

Miller, D.B., Feddes, R.G., 1971. "Global Atlas of Relative Cloud Cover." U.S. Nat'l Envr. Sat. Serv. And USAF Envr. Tech. Appl. Cntr., AD 739434 – Rep. No. 1, Washington, DC., 14 pp. plus charts.

Morcrette, J.-J., 2002a: Assessment of the ECMWF model cloudiness and surface radiation fields at the ARM-SGP site. *Mon. Wea. Rev.*, **130**, 257-277.

Morcrette, J.-J., 2002b: The surface downward longwave radiation in the ECMWF forecast system. *J. Climate*, **15**, 1875-1892.

Newman, M., Sardeshmukh, P.D., Bergman, J.W., 2000: An Assessment of the NCEP, NASA, and ECMWF Reanalyses over the Tropical West Pacific Warm Pool. *Bul. Amer. Meteor. Soc.*, **81**, 41–48.

Pan, H. L., and L. Mahrt, 1987: Interaction between soil hydrology and boundary layer development. *Bound.-Layer Meteor.,* **38,** 185–220.

Parrish, D. F., Derber, J. C., 1992: The National Meteorological Center's spectral statistical interpolation analysis system. *Mon. Wea. Rev.,* **120,** 1747–1763.

Randel, W., Udelhofen, P., Fleming, E., Geller, M., Gelman, M., Hamilton, K., Daroly, D., Ortland, D., Pawson, S., Swinbank, R., Wu, R., Baldwin, M., Chanin, M.-L., Keckhut, P., Labitzke, K., Remsberg, R., Simmons, A., Wu, D., 2004. The SPARC intercomparison of middle-atmosphere climatologies. *J. Climate*, **17**, 986-1003.

Rayner, N. A., Parker, D. E., Horton, E. B., Folland, C. K., Alexander, L. V., Rowell, D. P., Kent, E. C., Kaplan, A. 2003. Global analyses of sea surface temperature, sea ice and night marine air temperature since the late nineteenth century. *J. Geophys. Res.*, **108,** 4407.

Renwick, J. A., 2004. Trends in the Southern Hemisphere polar vortex in NCEP and ECMWF reanalyses, Geophys. Res. Lett., 31, L07209, doi:10.1029/2003GL019302.

Reynolds, R. W., Rayner, N. A., Smith, T. M., Stokes, D. C., Wang, W. 2002. An improved *in situ* and satellite SST analysis for climate. *J. Climate*, **15,** 1609–1625.

Serreze, M.C., Ciaran M. Hurst, C.M.,. 2000. Representation of Mean Arctic Precipitation from NCEP–NCAR and ERA Reanalyses. *J. Climate*.**13**, 182–201.

Simmons, A.J., Burridge, D.M., 1981. An energy and angular-momentum conserving vertical finite difference scheme and hybrid vertical coordinates. *Mon. Wea. Rev*., **109**, 758-766.

Simmons, A. J.; Jones, P. D.; da Costa Bechtold, V.; Beljaars, A. C. M.; Kållberg, P. W.; Saarinen, S.; Uppala, S. M.; Viterbo, P.; Wedi, N. 2004. Comparison of trends and low-frequency variability in CRU, ERA-40, and NCEP/NCAR analyses of surface air temperature. *J. Geophys. Res.,* 109, D24115, doi:10.1029/2004JD005306.

Sterl, A., 2004. On the (in)homogeneity of reanalysis products. *J. Climate*, **17,** 3866–3873

Tiedtke, M., 1989: A comprehensive mass flux scheme for cumulus parameterization in large-scale models. *Mon. Wea. Rev.,* **117,** 1779–1800.

Trenberth, K. E., Smith, L., 2005: The Mass of the Atmosphere: a Constraint on Global Analyses. *J. Climate*, **18**, 864-875.

Trenberth, K. E., Stepaniak, D. P. Caron, J. M., 2002: Accuracy of atmospheric energy budgets. *J. Climate*, **15**, 3343-3360.

Trenberth, K. E., Stepaniak, D. P., Hurrell, J. W., Fiorino, M., 2001: Quality of reanalyses in the tropics. *J. Climate*, **14**, 1499–1510.

Uppala, S.M., Kållberg, P.W., Simmons, A.J., Andrae, U., da Costa Bechtold, V., Fiorino, M., Gibson, J.K., Haseler, J., Hernandez, A., Kelly, G.A., Li, X., Onogi, K., Saarinen, S., Sokka, N., Allan, R.P., Andersson, E., Arpe, K., Balmaseda, M.A., Beljaars, A.C.M., van de Berg, L., Bidlot, J., Bormann, N., Caires, S., Chevallier, F., Dethof, A., Dragosavac, M., Fisher, M., Fuentes, M., Hagemann, S., Hólm, E., Hoskins, B.J., Isaksen, L., Janssen, P.A.E.M., Jenne, R., McNally, A.P., Mahfouf, J.-F., Morcrette, J.-J., Rayner, N.A., Saunders, R.W., Simon, P., Sterl, A., Trenberth, K.E., Untch, A., Vasiljevic, D., Viterbo, P., Woollen, J. 2005: The ERA-40 re-analysis. *Quart. J. R. Meteorol. Soc.*, **131**, 2961-3012.

van den Hurk, B.J.J.M., Viterbo, P., Beljaars, A.C.M., Betts, A.K., 2000. Offline validation of the ERA-40 surface scheme, ECMWF Tech Memo 295. (available from http://www.ecmwf.int/publications/library/do/references/lis/)

Viterbo, P., Beljaars, A., 1995. An improved land surface parameterization scheme in the ECMWF model and its validation. *J. Climate*, **8**, 2716-2748.

Webster, P., Holton, J., 1982, Cross equatorial response to middle latitude forcing in a zonally varying basic state. *J. Atmos. Sci.*, **39**, 722-733.

Xie, P., Arkin, P., 1996. Analyses of global monthly precipitation using gauge observations, satellite estimates, and numerical model predictions. *J. Climate,* **9,** 840–858.

Yang S.-K., Hou, Y.-T., Miller A. J., Campana K. A., 1999. Evaluation of the Earth radiation budget in NCEP–NCAR Reanalysis with ERBE. *J. Climate*,**12**, 477–493. DOI: 10.1175/1520-0442.

Appendix
List of acronyms and abbreviations used

3DVAR	3-dimensional variational analysis
AMIP	Atmospheric Model Intercomparison Project
AMSU	Advanced Microwave Sounding Unit
DJF	December through February average
DOE	United States Department of Energy
ECMWF	European Centre for Medium-Range Weather Forecasts
ERA-40	Second generation ECMWF reanalysis
FGAT	First guess at appropriate time (applies to 3DVAR)
HIRS	High-resolution Infrared Spectrometer
ICZ	Intertropical Convergence Zone
JJA	June through August average
KE	Kinetic energy
LHF	Surface latent heat flux
MRF	NCEP medium range forecast model.
MSE	Moist static energy
MSU	Microwave Sounding Unit
N	North (latitude)
NCAR	National Center for Atmospheric Research
NCEP	National Centers for Environmental Prediction
NCL	NCAR command language
NDRa2	NCEP-DOE Reanalysis II
NESDIS	National Environmental Satellite, Data and Information Service
NNRa1	NCEP-NCAR Reanalysis
NSDIC	National Snow and Ice Data Center
OI	Optimal interpolation
P	Precipitation rate
PAOB	Pseudo Surface Pressure Observations (Australian sea level bogus data)
q	Specific humidity
rmse	root mean squared error
S	South (latitude)
SBUV	Solar Backscattered Ultra Violet
SHF	Surface sensible heat flux
slwrf	Surface thermal radiative flux downwards
SLP	Sea level pressure
SNYOP	Surface Synoptic Observation
SPCZ	South Pacific Convergence Zone
sswrf	Surface solar radiative flux downwards
SSU	Stratospheric Sounding Unit
SSM/I	Special Sensor Microwave/Imager
TCWV	Total column water vapor
TOA	Top of atmopshere
TOAlwrf	Top of atmosphere longwave radiative flux upward
TOAswrf	Top of atmosphere solar radiative flux downward

TOVS	Operational Vertical Sounder and the Television Infrared Operational Satellite
T	Temperature
Tn	Triangular spectral truncation at order n
TOMS	Total ozone Mapping Spectrometer
U	Zonal wind component
USAF	United States Air Force
V	Meridional wind component
VTPR	Vertical Temperature Profile Radiometer
Z	Geopotential height
ω	Pressure velocity
[a]	Zonal average of variable a
{a}	Global horizontal average

Figure Captions

Fig. 1. Net downward shortwave radiative flux at the top of the atmosphere during December-February (DJF, left column) and June-August (JJA, right column) for the 22 year period 1979-2000. (Net is downward minus upward reflected solar radiation.) Top row: solid line NDRa2 [TOAswrf] data, dashed line ERA-40 data. Middle row: ERA-40 minus NDRa2 [TOAswrf] difference. Bottom row: geographical distribution of the TOAswrf difference: ERA-40 minus NDRa2 data with contour interval of 20; negative values shaded. Units are W m^{-2}. Notable differences occur near the ICZ and SPCZ and polar ice sheets of the summer hemisphere.

Fig. 2. Similar to fig. 1, except showing longwave upward radiative flux at the top of the atmosphere. Units are W m^{-2} and contour interval is 10 W m^{-2}. Large differences (up to 25%) occur near much of the ICZ and SPCZ.

Fig. 3. Similar to fig. 1, except showing short wave radiative flux reaching the surface. Units are W m^{-2} and contour interval is 20 W m^{-2}. Notable differences occur near the ICZ and SPCZ and high latitudes of the summer hemisphere.

Fig. 4. Similar to fig. 1, except showing surface longwave radiative flux. Units are W m^{-2} and contour interval is 10 W m^{-2}. Notable differences occur near higher topography and polar land areas. Winter subtropical oceans have uniformly larger slwrf in NDRa2 data.

Fig. 5. Zonal mean temperature, [T] in ERA-40 data (top row) and difference: ERA-40 minus NDRa2 (middle row). Geographic distribution of the T difference at 150 hPa, bottom row. Left column DJF, right column JJA. Contour interval is 10 K for top and 1 K for middle and bottom rows. Negative values (ERA-40 cooler) are shaded. Tropical tropopause and lower level Southern Hemisphere midlatitudes are colder in ERA-40 data. The difference near tropopause level is mainly over subtropical oceans.

Fig. 6. Similar to fig. 5 except showing zonal mean zonal wind, [U]. ERA-40 has equatorial, upper tropospheric westerlies not seen in other datasets during DJF. Larger

differences occur in the stratosphere, where ERA-40 data often have stronger easterlies in middle stratosphere, weaker near equatorial tropopause. Stratospheric winter polar night jet is stronger in ERA-40 data. Contour interval is 5 m/s for top and middle row, 1 m/s for bottom row. Shaded areas indicate negative values (easterlies).

Fig. 7. Geographic distribution of zonal wind difference, ERA-40 minus NDRa2 at 150 hPa for DJF (top) and JJA (bottom). Contour interval is 1 m/s. Shaded areas are where the difference is negative. Larger differences occur over the tropical Atlantic and eastern tropical Pacific. In DJF, NDRa2 data have stronger easterlies over Atlantic and across Indian oceans; in ERA-40, region of westerlies is wider longitudinally in tropical Atlantic.

Fig. 8. Similar to the left column of fig. 5, except for zonal mean cross sections of pressure velocity ($\omega = dP/dt$). Contour interval is 0.01 Pa/s for top and middle plot, 0.005 for the difference field (bottom plot); shaded areas indicate negative values (upward motion). ERA-40 has a "second" peak rising zone near 5 N in [ω] that is not apparent in NDRa2 data.

Fig. 9. Comparison plots of time mean pressure velocity ($\omega = dP/dt$) for NDRa2 data (top row) and ERA-40 data (bottom row) during DJF (left column) and JJA (right column). Despite using the same grid, the NDRa2 data tend to have broader features such as parts of the ICZ. NDRa2 data have very weak ICZ in the central Atlantic and weaker ICZ in the east Pacific than ERA-40 during DJF. The Atlantic and east Pacific ICZ is at a higher latitude than many other regions, consequently, ERA-40 data have the 'second' peak rising zone mentioned in previous figure. Near steep-sloped topographic features, such as the Himalayas and the Andes ω has more waviness in ERA-40 data. Contour interval is 0.03 Pa/s; shaded areas indicate negative values (upward motion).

Fig. 10. Similar to fig. 5 except using vectors to show the zonal mean circulation in the meridional and vertical plane.

Fig. 11. Zonal mean specific humidity [q] ERA-40 data top row, [q] difference: ERA-40 minus NDRa2 middle row, bottom row is difference in q, ERA-40 minus NDRa2 at 700 hPa level. Left column DJF, right column JJA. Contour interval is 1 gm/kg for top and bottom rows, 0.2 gm/kg middle row. Negative values are shaded. Distribution of [q] for NDRa2 very similar in appearance to top row. ERA-40 has higher q than NDRa2 along most of the ICZ, lower in much of the winter hemisphere subtropics.

Fig. 12. Similar to fig. 1 except showing precipitation rate, P. Units are mm/day and the contour interval is 2 mm/day. ICZ in Atlantic and eastern Pacific has greater P in ERA-40.
In contrast, NDRa2 data has larger ICZ-associated P in Indian and west Pacific oceans. During winter, P in midlatitude storm tracks is generally less in ERA-40. During JJA, less P in ERA-40 over northern continents.

Fig. 13. Zonal mean surface sensible heat flux, [SHF] and ERA-40 minus NDRa2 difference (top and second row, respectively). Zonal mean surface latent heat flux, [LHF] and ERA-40 minus NDRa2 difference (third and bottom row, respectively). In top and third rows: solid line is NDRa2; dashed line is ERA-40. Units are W m^{-2}.

Fig. 14. Similar to fig. 5 except for moist static energy, MSE. Contour interval is 20 000 m^2 s^{-2} for the top row and 1000 m^2 s^{-2} for the middle row. The bottom row shows MSE at 850 hPa with contour interval 2000 m^2 s^{-2}. Low level tropical differences reflect greater moisture present in ERA-40 data, especially along the ICZ. Tropical tropopause and southern hemisphere low level midlatitudes regions differences reflect cooler ERA-40 temperatures there.

Fig. 15. Similar to fig. 5 except for kinetic energy, KE. Contour interval is 200 m^2 s^{-2} for the top row and 25 m^2 s^{-2} for the middle row. The bottom row shows KE at 200 hPa with contour interval 25 m^2 s^{-2}. ERA-40 data generally have more [KE] especially in winter stratosphere, winter subtropical jet, and tropical stratosphere.

Table 1. Some aspects of the NDRa2 and ERA-40 input data Note: not all data were available during the full length of the assimilated period. See the original references for details. Acronyms and abbreviations are defined in the appendix.

Dataset	**NDRa2**	**ERA-40**
Primary reference	Kanamitsu et al. (2002)	Uppala et al. (2005)
Input Data		
Satellite data:	NESDIS TOVS temperature retrievals, Cloud track winds. (No moisture data used)	Direct assimilation of VTPR, TOVS (HIRS, MSU, SSU) and AMSU-A Level-1c radiances, Atmospheric Motion Vectors, scatterometer winds, SSM/I radiances as 1D-Var retrievals of TCWV and surface wind speed TOMS and SBUV data in ozone analysis, Altimeter wave height data (see Hernandez et al., 2004)
Upper air data	Radiosondes, dropsondes, pibals, aircraft data, wind profilers	Radiosondes, dropsondes, pibals, aircraft data, wind profilers
Surface data (snow cover)	Stations, ships, buoys, PAOBs, (NSIDC-based, USAF snow cover after fall 1998, depth is dynamic)	Stations, ships, buoys, PAOBs. (SYNOP snow depth, most after 1976)
SST and Sea Ice	AMIP-II (should be same as ERA-40 except for time interpolation, Kanamitsu, pers. comm., 2007), Reynolds SST after 1999	Reynolds et al. (2002), Rayner et al. (2003) and other NCEP products
Period	1979- present	September 1957-August 2002 (45 years)

Table 2. Some aspects of the NDRa2 and ERA-40 assimilation systems. Acronyms and abbreviations are defined in the appendix.

Dataset	**NDRa2**	**ERA-40**
Primary reference	Kanamitsu et al. (2002)	Uppala et al. (2005)
Period	1979- present	September 1957-August 2002 (45 years)
Assimilation model		
Model based on:	MRF (ca 1995, with modifications) full radiation calculation hourly	ECMWF forecast model CY23r4 (operational in June 2001)
Assimilation scheme	3DVAR (Parrish and Derber, 1992)	3DVAR-FGAT, OI for surface parameters and ocean wave height
Horizontal type, resolution (grid type, in latitude x longitude)	Spectral, T62 (Gaussian, 94 x 192 for dynamics and physics)	Spectral, T159 (linear reduced Gaussian grid 160 by up to 320, declining for latitudes >27^o), (Hortal and Simmons, 1991)
Vertical coordinate type, number of levels	Sigma, 28	Hybrid sigma (Simmons and Burridge, 1981), 60
Horizontal grid, levels used here	2.5^o latitude by 2.5^o longitude, 17 levels	2.5^o latitude by 2.5^o longitude, 17 levels
Parameterizations		
Orography	Smoothed mean orography to remove Gibbs oscillations.	Smoothed mean orography
Land surface	Pan and Mahrt (1987), Mahrt and Pan (1984) Soil moisture correction based on model minus observed precipitation	Viterbo and Beljaars (1995) Van den Hurk et al (2000)
PBL	Hong and Pan (1996)	Beljaars and Viterbo (1998), Viterbo et al. (1999)
Radiation	Chou (1992), Chou and Lee (1996) (shortwave) Fels and Schwarztkopf (1975) (longwave)	Morcrette et al (2002a), (shortwave), Morcrette et al (2002b), (longwave) See also Gregory et al. (2000)
Time varying radiatively active: gases / aerosols (i.e. volcanic eruptions)	No (CO_2 constant) / No	Yes (CO_2, CH_4, N_2O, CFC-11, CFC-12, based on Houghton, et al., 1996) / No
Convection	Simplified Arakawa Schubert, Grell (1993)	Tiedtke (1989) type, see Gregory et al. (2000)
Data Sources:		
NDRa2: http://nomad3.ncep.noaa.gov/ncep_data/index.html ERA-40: http://data.ecmwf.int/data/d/ERA-40_mnth/		

Table 3 Selected Differences between NDRa2 and ERA-40 radiation variables.

Variable	Location	Season	Difference: ERA-40 – NDRa2
[TOAswrf]	Summer polar regions >70^{o}	DJF,JJA	+20, +20 to +40 W/m^2
	ICZ	JJA	+30 W/m^2
TOAswrf	NW tropical Pacific	JJA	- 20 to -40 W/m^2
	South of: Atlantic ICZ and E Pacific ICZ	DJF,JJA	+20 to +30 W/m^2
	SPCZ	DJF	- 20 to -40 W/m^2
TOAlwrf	NW tropical Pacific, S tropical Indian Ocean	JJA	-20 to -60 W/m^2
	S tropical Indian, SW tropical Pacific, SPCZ	DJF	-20 to -40 W/m^2
	SPCZ	JJA	-10 to -40 W/m^2
[sswrf]	40N to 90N	JJA	-30 to -100 W/m^2
	60S to 70S	DJF	-30 to -40 W/m^2
sswrf	Sahara and Arabia	DJF,JJA	+20 to +40 W/m^2
	High topography (Tibet, Rockies, Andes)	DJF,JJA	-40 to -80 W/m^2 (even larger during summer)
	NW tropical Pacific, S tropical Indian Ocean	JJA	-20 to -60 W/m^2
	S tropical Indian, SW tropical Pacific, SPCZ	DJF	-20 to -40 W/m^2
[slwrf]	Summer polar regions > 65^{o}	JJA	+20 to +45 W/m^2
slwrf	High topography (Tibet, Rockies, Andes)	DJF,JJA	+30 to +100 W/m^2
	Sahara	JJA	+20 to +30 W/m^2

Table 4 Selected Differences between NDRa2 and ERA-40 in Temperature

Variable	Location	Elevation	Season	Difference: ERA-40 – NDRa2
[T]	20S to 20N	near 100 hPa	DJF,JJA	-2 to -3 K
	90S to 30S	10 hPa	JJA	-2 to -5 K
	90S to 70S	300 to 200 hPa	DJF,JJA	-1 to -3 K
T	Sahara	925 hPa	DJF,JJA	+2 to +3 K
	Subtropical ocean: 20S to 40S	150 hPa	DJF,	-2 to -3 K,
	Subtropical and tropical ocean: 0S to 30S	150 hPa	JJA	-2 to -3 K
	Subtropical ocean: 20N to 40N	150 hPa	JJA	-2 to -3 K
	Some eastern subtropical ocean stratus regions	925 hPa	JJA	+2 K

Table 5 Selected Differences between NDRa2 and ERA-40 mass fields

Variable	Location	Elevation	Season	Difference: ERA-40 – NDRa2
[SLP]	75S to 90S		DJF,JJA	-4 to -6, -8 to -12 hPa
SLP	Antarctica		DJF,JJA	0 to -12, 0 to -26 hPa
	Greenland		DJF	0 to -4 hPa
[Z]	40S to 20N	20 to 100 hPa	DJF,	-60 m
	30S to 20N	10 to 100 hPa	JJA	-60 m
	Winter pole	10 to 50 hPa	DJF,JJA	-60 to -160 m
Z	Ocean areas, except Arctic	150 hPa	JJA	Most areas -40m or more
	50S to 90S	500 hPa	DJF,JJA	Only region with -20 (ocean) and +20 m areas (continent)

Table 6 Selected Differences between NDRa2 and ERA-40 velocity fields

Variable	Location	Elevation	Season	Difference: ERA-40 – NDRa2
[U]	10S to 0	150 to 300 hPa	DJF	+2 to +3 m/s (sign reversal)
	10N to 30N	30 to 100 hPa	DJF	-3 to -4 m/s,
	10S to 0	70 hPa	JJA	+2 m/s
	35S to 20S	10 to 100 hPa	JJA	-2 to -4 m/s
	10S to 10N	30 hPa	JJA	-4 to -7 m/s
U	Eastern Pacific (20S to 0, 140W to 70W)	150 hPa	DJF,	+3 to +9 m/s,
	S tropical Atlantic (20S to 5S, 30W to 20E)	150 hPa	DJF,	+2 to +4 m/s,
	0 to 10N, 70W to 40W	150 hPa	JJA	-2 m/s
	S subtropical Indian Ocean (30S, 70E to 100E)	150 hPa	DJF,JJA	+2 to +3 m/s, +3 to +4 m/s
[V]	0 to 15N 0 to 10N	200 to 300 hPa 500 to 700 hPa	DJF	+0.4 to +0.7 m/s -0.3 to -0.4 m/s
	10S to 5N	300 hPa 500 to 700 hPa	JJA	-0.4 to -1.0 m/s +0.4 to +0.6 m/s
V	Amazonia (5S to 5N, 60W to 40W)	300 hPa	DJF	> +2 m/s
	5S to 5N, 10E to 20E	300 hPa	DJF	> +2 m/s
	5N, 120W to 75W	700 hPa	DJF	-1 m/s
	10N to 20N, 45E to 65E	700 hPa	DJF	+1.5 to +2 m/s
	Equatorial Africa (5S to 10N, 0 to 30E)	700 hPa	JJA	+1 to +4 m/s
	East tropical Pacific (15S to 5N, 110W to 60W)	300 hPa	JJA	-1 to -2.5 m/s
	15S to 5N, 20W to 30E	300 hPa	JJA	-1.5 to -4.5 m/s
	Near (5N, 80E)	300 hPa	JJA	+2.5 m/s
[ω]	Near 5N	250 to 850 hPa	DJF,JJA	-0.01 to -0.02 Pa/s, -0.01 Pa/s
ω	ICZ over Atlantic, central and western Pacific	500 hPa	DJF	-0.02 to -0.06 Pa/s
	ICZ over Indian Ocean	500 hPa	DJF	+0.02 to +0.04 Pa/s
	Near W & central Pacific ICZ (10N,130E) to (0, 150W)	500 hPa	JJA	+0.02 to +0.04 Pa/s

Table 7 Selected Differences between NDRa2 and ERA-40 moisture-related fields

Variable	Location	Elevation (if applicable)	Season	Difference: ERA-40 – NDRa2
[q]	15S to 10N	400 to 925 hPa	DJF	+0.4 to +0.8 gm/kg
	15N to 45N	700 to 1000 hPa	DJF	-0.3 to -0.8 gm/kg
	5N to 25N	400 to 925 hPa	JJA	+0.4 to +0.8 gm/kg
	30N to 40N	850 to 1000 hPa	JJA	-0.6 to -1.4 gm/kg
q	Indian and Atlantic Ocean and African ICZ, tropical SPCZ	700 hPa	DJF	>1 gm/kg
	Indian and Pacific Ocean ICZ, tropical SPCZ	850 hPa	DJF	>1 gm/kg
	Tibetan Plateau	700 to 850 hPa	DJF,JJA	Up to -7, -12 gm/kg
[P]	Near 5N		DJF	Up to +2.6 mm/day
	30N to 40N		DJF	-0.6 to -0.8 mm/day
	40S to 30S		JJA	-0.8 to -1.0 mm/day
	Near 5S		JJA	+1.2 mm/day
	Near 3N		JJA	-1 mm/day
	Northern midlatitudes		JJA	-0.2 to -0.7 mm/day
P	Atlantic and Pacific ICZ, tropical SPCZ		DJF	+2 to +6 mm/day
	Equatorial Indian Ocean		DJF	-2 to -4 mm/day
	Java region		DJF	+2 to +8 mm/day
	East Pacific ICZ		JJA	+2 to +4 mm/day
	West Pacific and Atlantic ICZ		JJA	-2 to -4 mm/day
	Isolated extrema: Sri Lanka, Thailand		JJA	-12 to -22 mm/day
	Isolated extrema: Central America, NW South America, New Guinea		JJA	+16 to +26 mm/day

Table 8 Selected Differences between NDRa2 and ERA-40 energy-related fields

Variable	Location	Elevation (if applicable)	Season	Difference: ERA-40 – NDRa2
{SHF}	Global mean		DJF,JJA	+8, +7 W/m^2
[SHF]	90S to 70S		DJF,JJA	+8 to +23, +22 to +34 W/m^2
	45N to 90N		DJF	+10 to +23 W/m^2
SHF	Sahara, Siberia, NW North America, SE Asia, S India, Patagonia, S Brazil		JJA	+20 to +60 W/m^2
	Arctic Ocean, W US, W Canada, Siberia, SE Asia, Sahara, N Brazil		DJF	+20 to +60 W/m^2
	Kuro Shio, Gulf Stream, GIN Sea		DJF	-20 to -60 W/m^2
{LHF}	Global mean		DJF,JJA	-7, -8 W/m^2
[LHF]	20S to 65N		DJF	-6 to -19 W/m^2
	15S to 5S, 50N to 70N		JJA	-15 to -21 W/m^2
LHF	Atlantic (5N to 10N, 50W to 10W)		DJF	-40 to -60 W/m^2
	Kuro Shio, Gulf Stream		DJF	-20 to -80 W/m^2
	S Brazil, Patagonia		DJF	-40 to -60 W/m^2
	Atlantic (10N, 55W to 55W to 35W)		JJA	-40 to -50 W/m^2
	Siberia, Alaska, Canada		JJA	-20 to -60 W/m^2
	S of W Pacific ICZ		JJA	-20 to -50 W/m^2
[KE]	Winter polar stratosphere poleward of 60^o	10 to 30 hPa	DJF,JJA	+100 to +250 m^2/s^2, +20 to +160 m^2/s^2
	Equatorial stratosphere (10S to 10N)	10 to 50 hPa	DJF,JJA	+50 to +300 m^2/s^2, +60 to +260 m^2/s^2
	S Hemis. subtropical jet (50S to 30S)	200 hPa	DJF,JJA	>+50 m^2/s^2, +40 to +100 m^2/s^2
KE	Winter subtropical jet maxima	200 hPa	DJF,JJA	100 to >+140 m^2/s^2, 175 to >+250 m^2/s^2
	Indian tropical easterly jet	200 hPa	JJA	-100 m^2/s^2

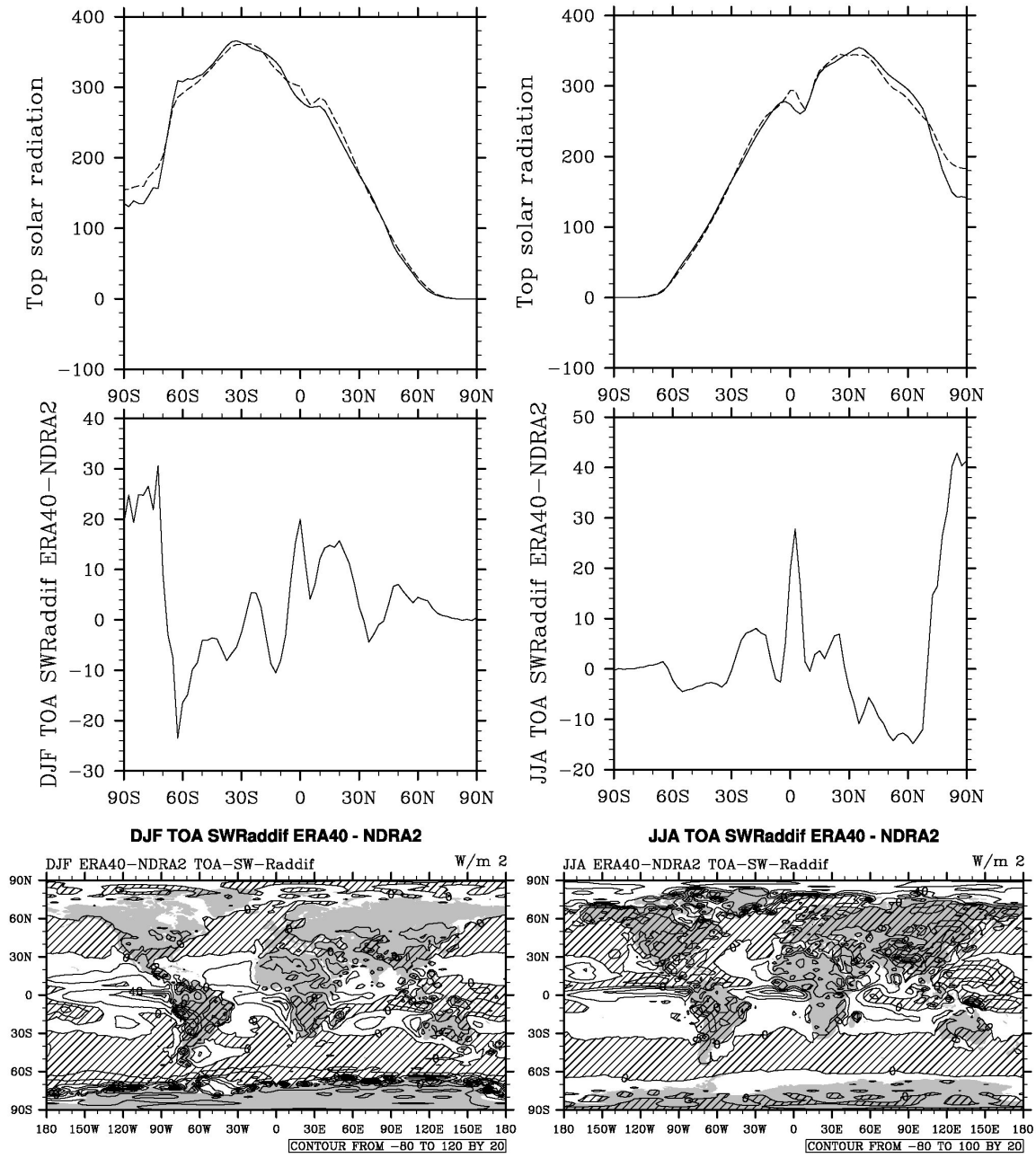

Fig. 1. Net downward shortwave radiative flux at the top of the atmosphere during December-February (DJF, left column) and June-August (JJA, right column) for the 22 year period 1979-2000. (Net is downward minus upward reflected solar radiation.) Top row: solid line NDRa2 [TOAswrf] data, dashed line ERA-40 data. Middle row: ERA-40 minus NDRa2 [TOAswrf] difference. Bottom row: geographical distribution of the TOAswrf difference: ERA-40 minus NDRa2 data with contour interval of 20; negative values shaded. Units are W m^{-2}. Notable differences occur near the ICZ and SPCZ and polar ice sheets of the summer hemisphere.

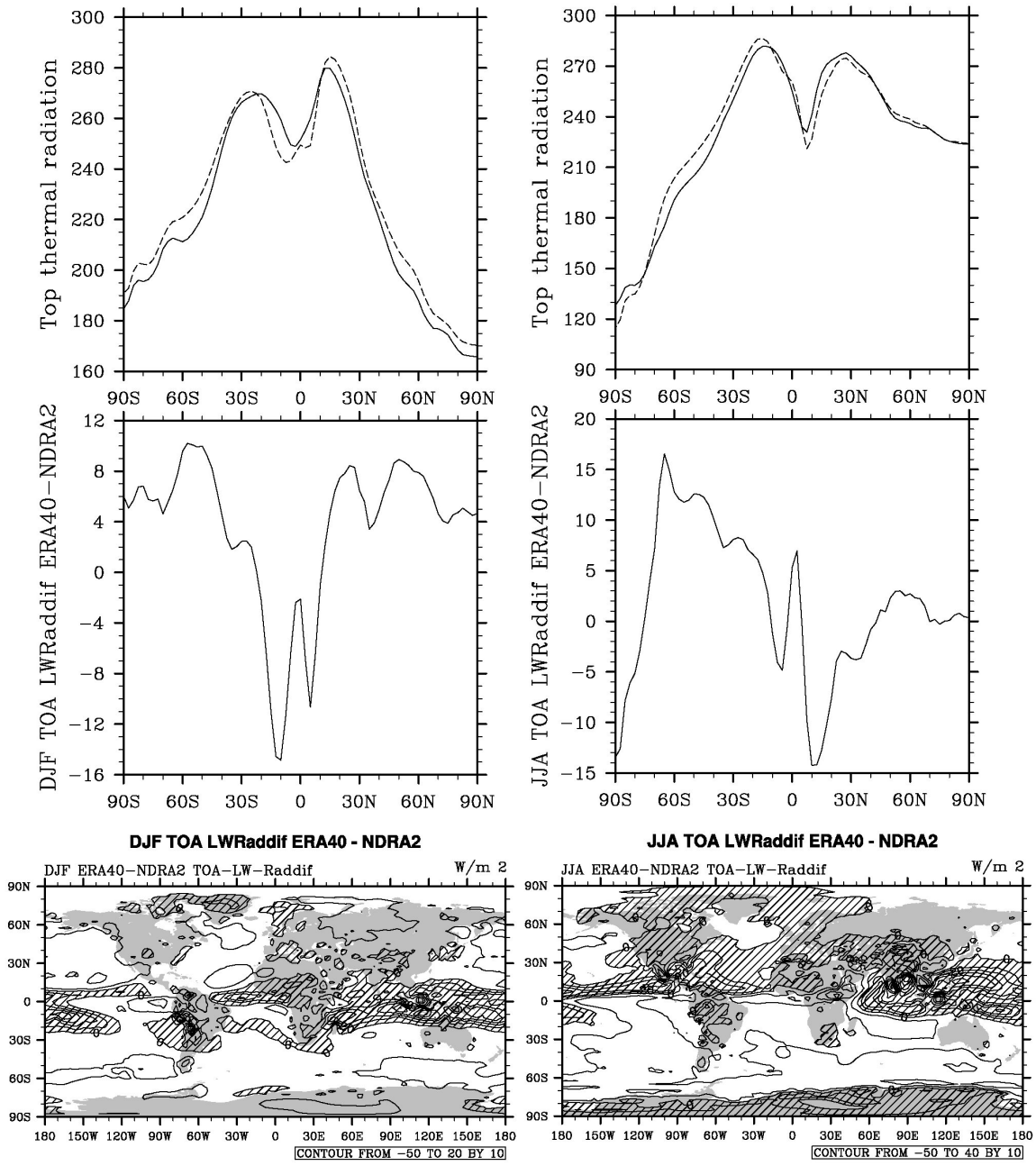

Fig. 2. Similar to fig. 1, except showing longwave upward radiative flux at the top of the atmosphere. Units are W m^{-2} and contour interval is 10 W m^{-2}. Large differences (up to 25%) occur near much of the ICZ and SPCZ.

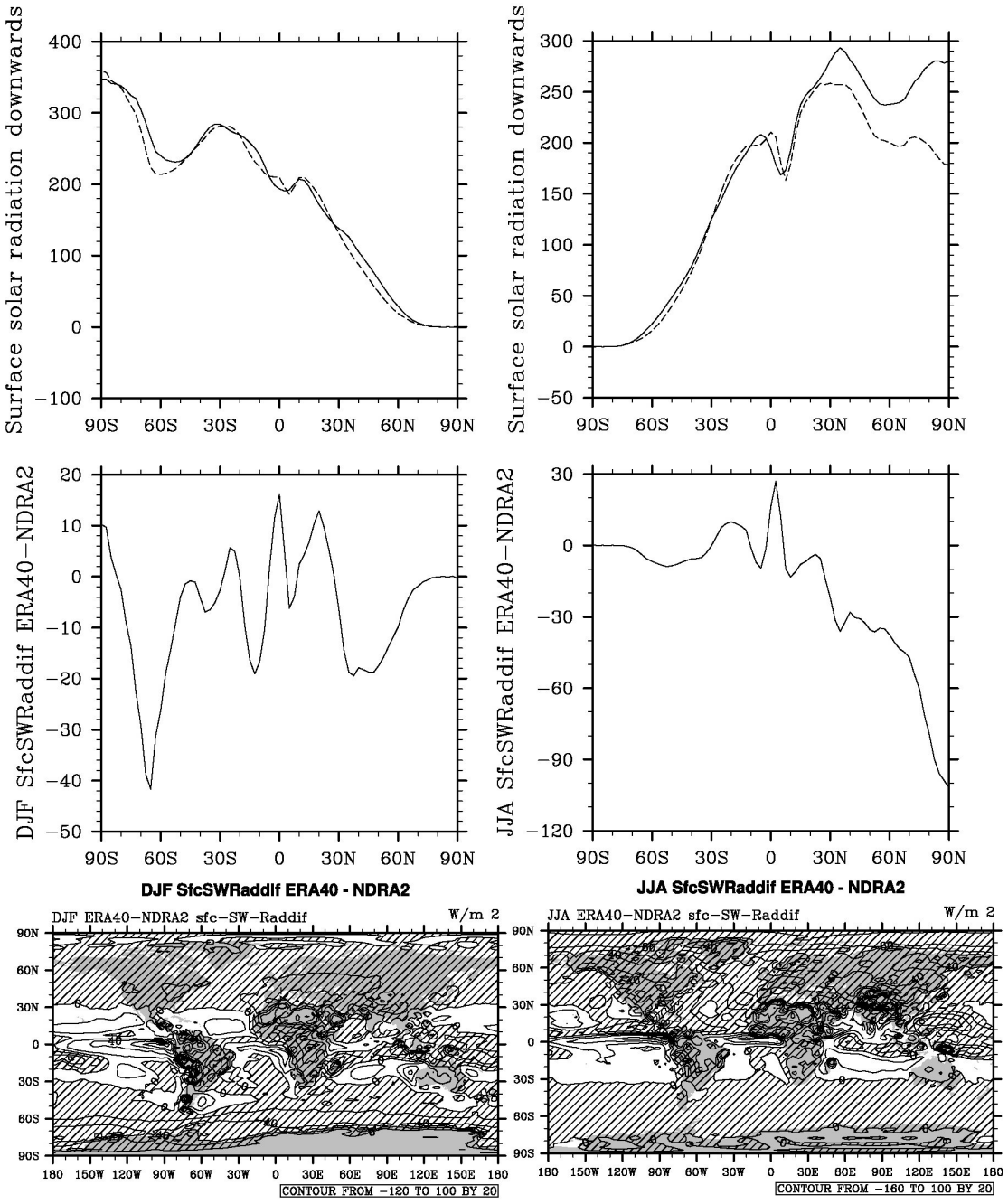

Fig. 3. Similar to fig. 1, except showing short wave radiative flux reaching the surface. Units are W m^{-2} and contour interval is 20 W m^{-2}. Notable differences occur near the ICZ and SPCZ and high latitudes of the summer hemisphere.

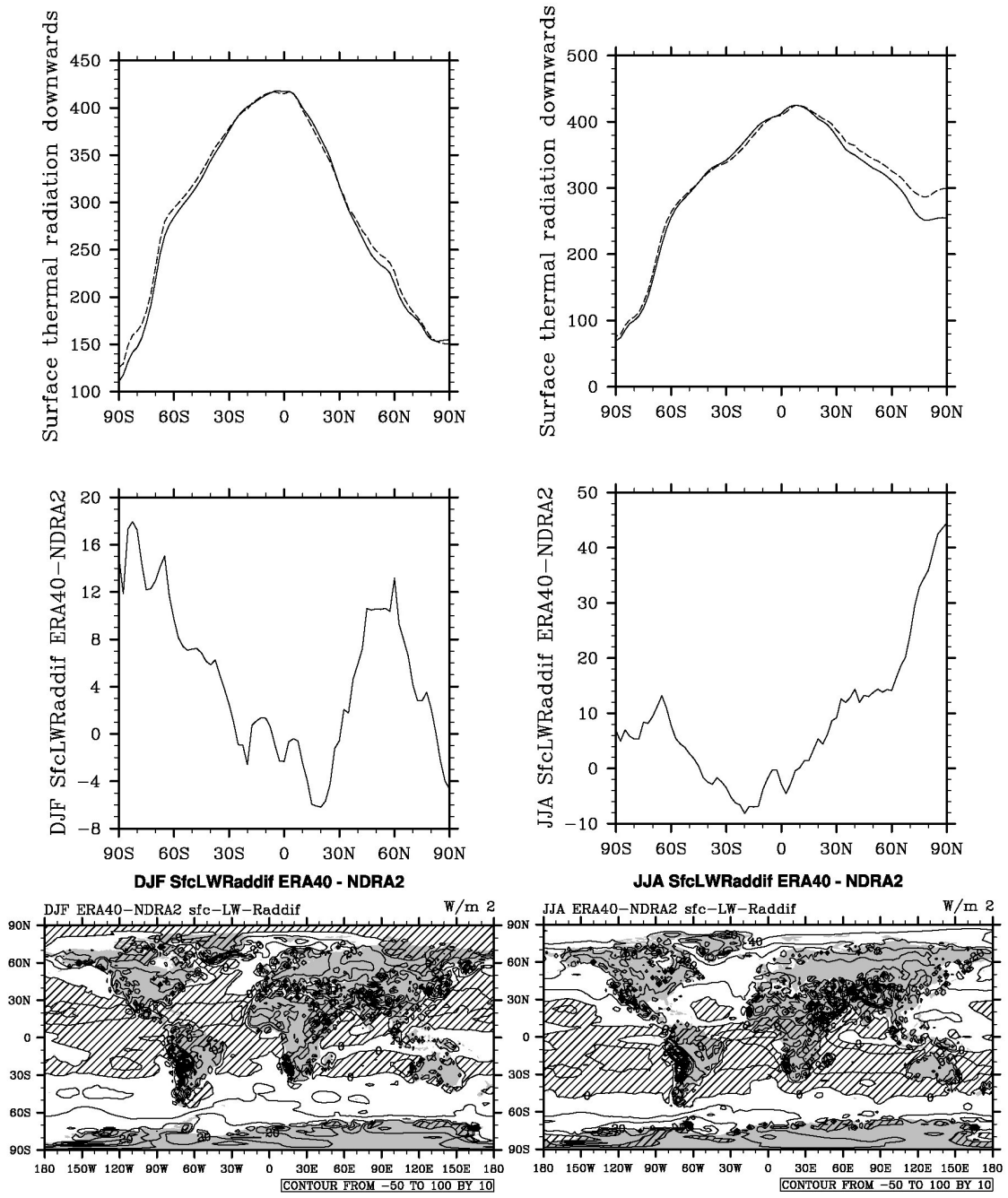

Fig. 4. Similar to fig. 1, except showing surface longwave radiative flux. Units are W m^{-2} and contour interval is 10 W m^{-2}. Notable differences occur near higher topography and polar land areas. Winter subtropical oceans have uniformly larger slwrf in NDRa2 data.

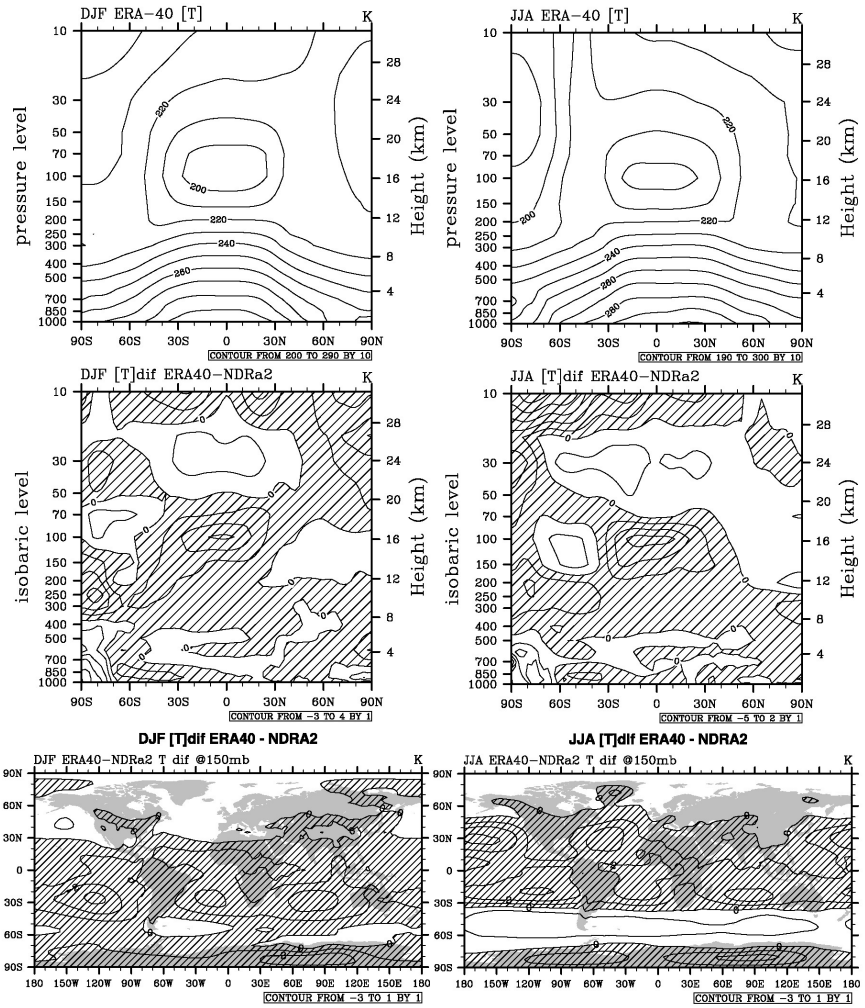

Fig. 5. Zonal mean temperature, [T] in ERA-40 data (top row) and difference: ERA-40 minus NDRa2 (middle row). Geographic distribution of the T difference at 150 hPa, bottom row. Left column DJF, right column JJA. Contour interval is 10 K for top and 1 K for middle and bottom rows. Negative values (ERA-40 cooler) are shaded. Tropical tropopause and lower level Southern Hemisphere midlatitudes are colder in ERA-40 data. The difference near tropopause level is mainly over subtropical oceans.

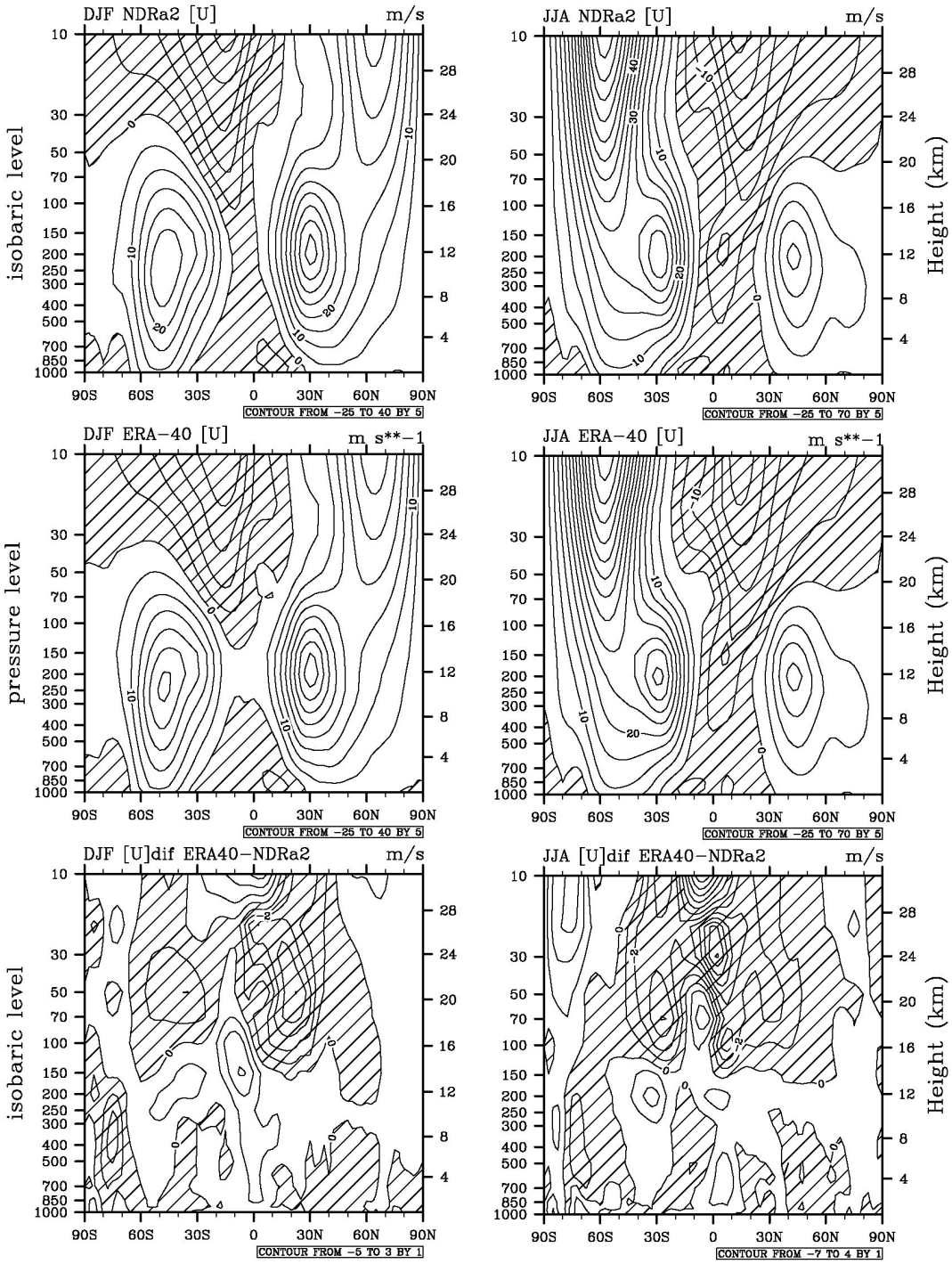

Fig. 6. Similar to fig. 5 except showing zonal mean zonal wind, [U]. ERA-40 has equatorial, upper tropospheric westerlies not seen in other datasets during DJF. Larger differences occur in the stratosphere, where ERA-40 data often have stronger easterlies in middle stratosphere, weaker near equatorial tropopause. Stratospheric winter polar night jet is stronger in ERA-40 data. Contour interval is 5 m/s for top and middle row, 1 m/s for bottom row. Shaded areas indicate negative values (easterlies).

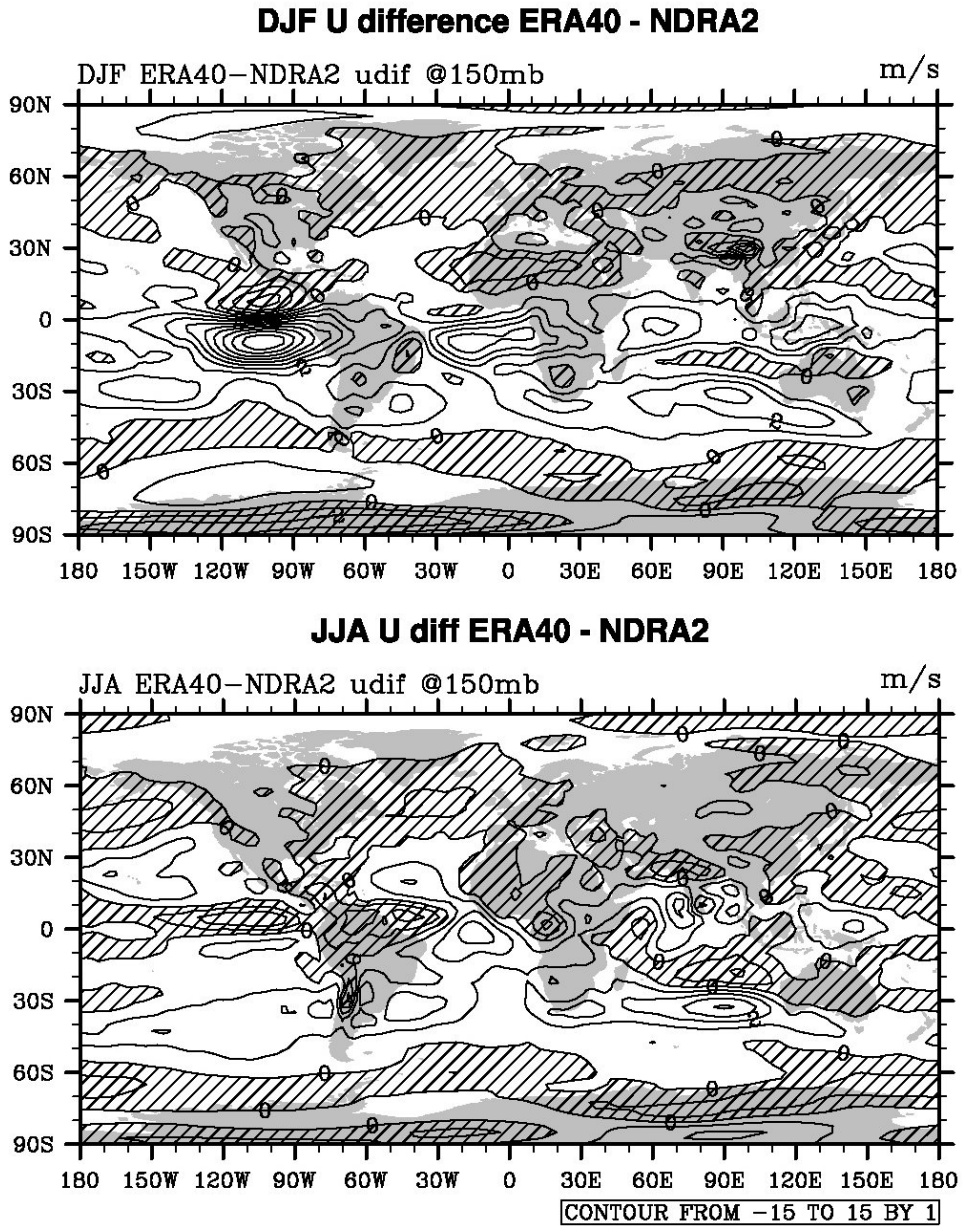

Fig. 7. Geographic distribution of zonal wind difference, ERA-40 minus NDRa2 at 150 hPa for DJF (top) and JJA (bottom). Contour interval is 1 m/s. Shaded areas are where the difference is negative. Larger differences occur over the tropical Atlantic and eastern tropical Pacific. In DJF, NDRa2 data have stronger easterlies over Atlantic and across Indian oceans; in ERA-40, region of westerlies is wider longitudinally in tropical Atlantic.

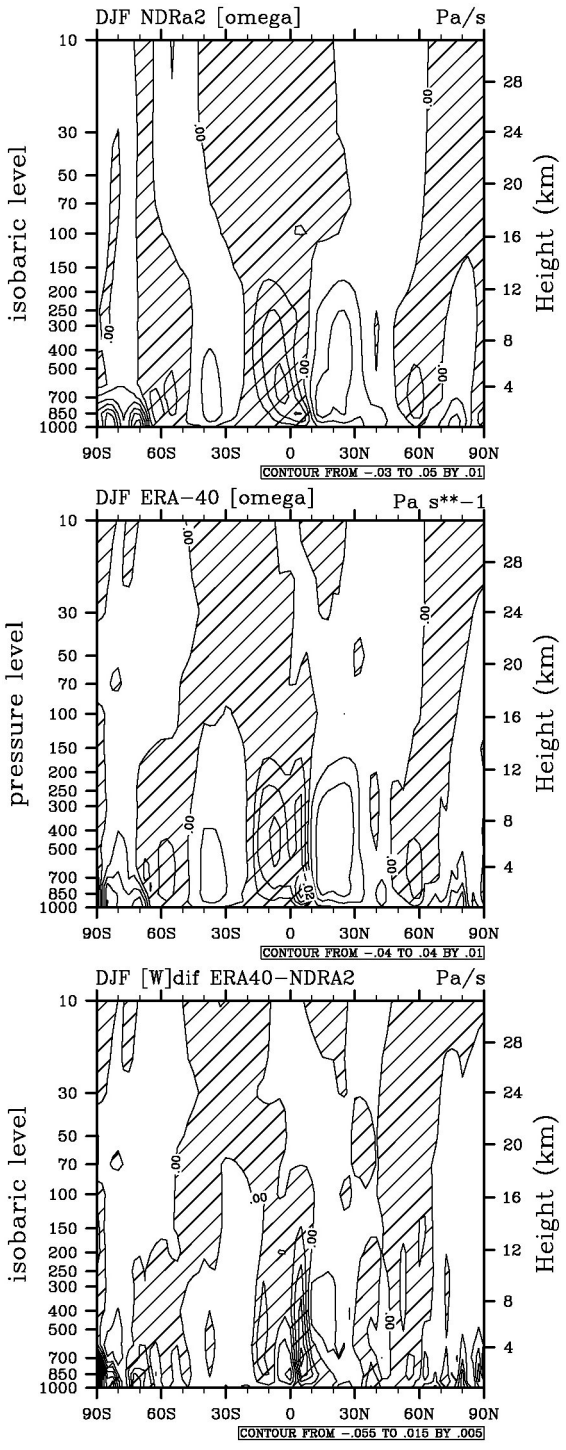

Fig. 8. Similar to the left column of fig. 5, except for zonal mean cross sections of pressure velocity (ω = dP/dt). Contour interval is 0.01 Pa/s for top and middle plot, 0.005 for the difference field (bottom plot); shaded areas indicate negative values (upward motion). ERA-40 has a "second" peak rising zone near 5 N in [ω] that is not apparent in NDRa2 data.

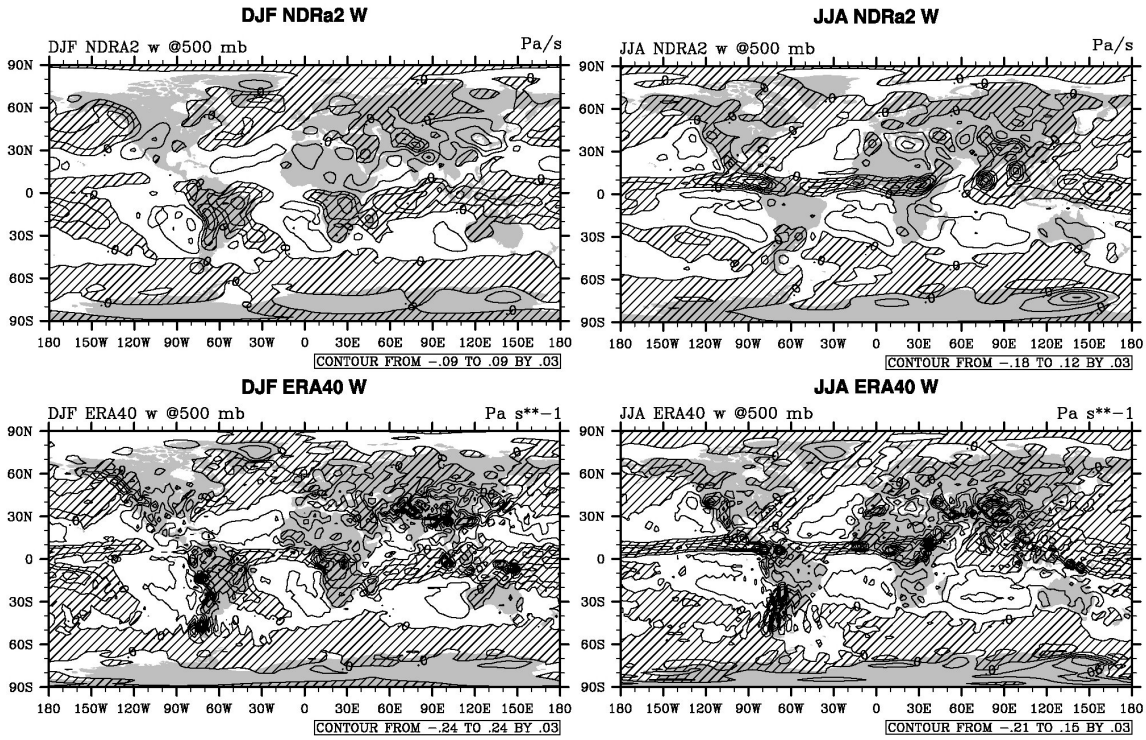

Fig. 9. Comparison plots of time mean pressure velocity (ω = dP/dt) for NDRa2 data (top row) and ERA-40 data (bottom row) during DJF (left column) and JJA (right column). Despite using the same grid, the NDRa2 data tend to have broader features such as parts of the ICZ. NDRa2 data have very weak ICZ in the central Atlantic and weaker ICZ in the east Pacific than ERA-40 during DJF. The Atlantic and east Pacific ICZ is at a higher latitude than many other regions, consequently, ERA-40 data have the 'second' peak rising zone mentioned in previous figure. Near steep-sloped topographic features, such as the Himalayas and the Andes ω has more waviness in ERA-40 data. Contour interval is 0.03 Pa/s; shaded areas indicate negative values (upward motion).

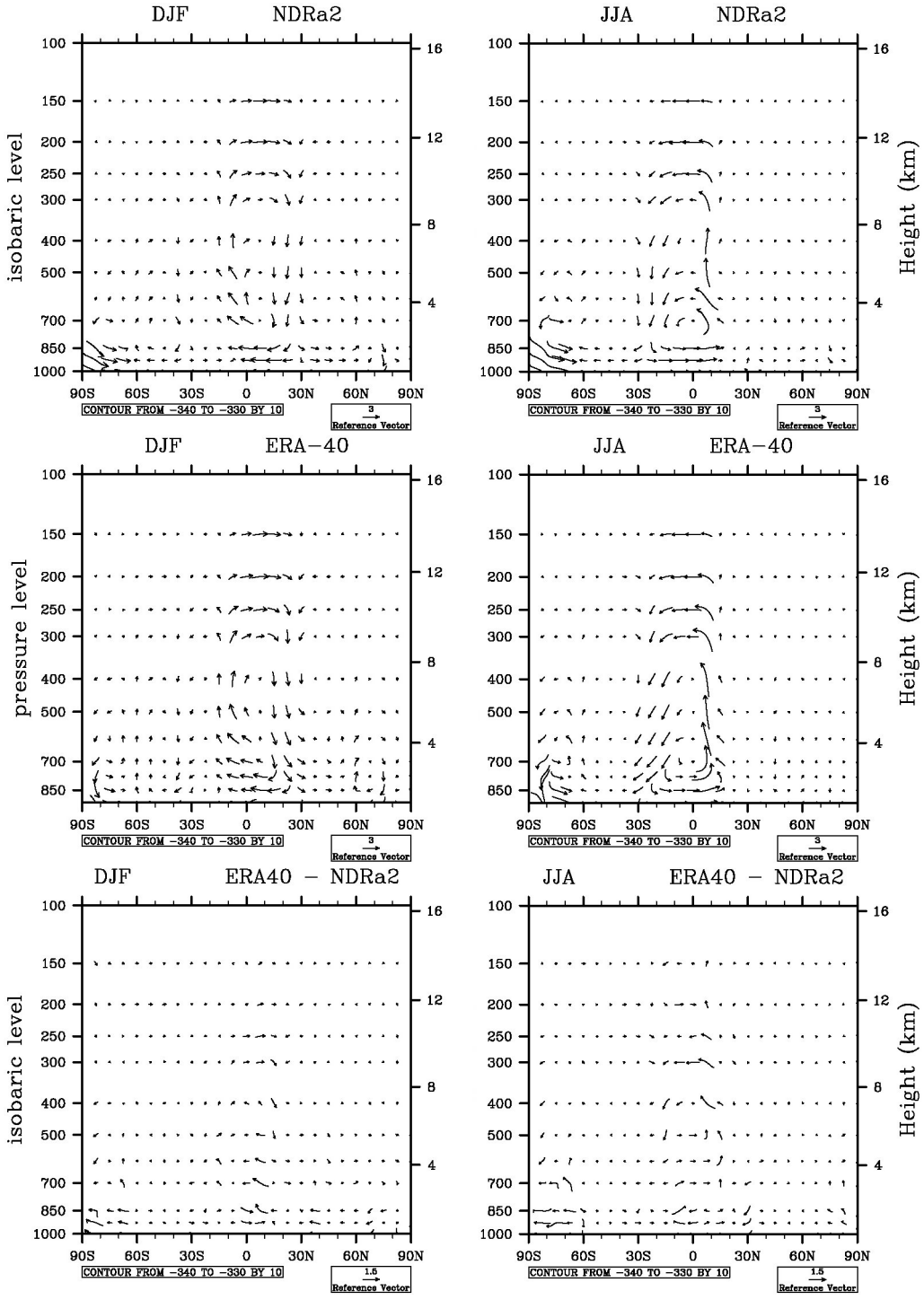

Fig. 10. Similar to fig. 5 except using vectors to show the zonal mean circulation in the meridional and vertical plane.

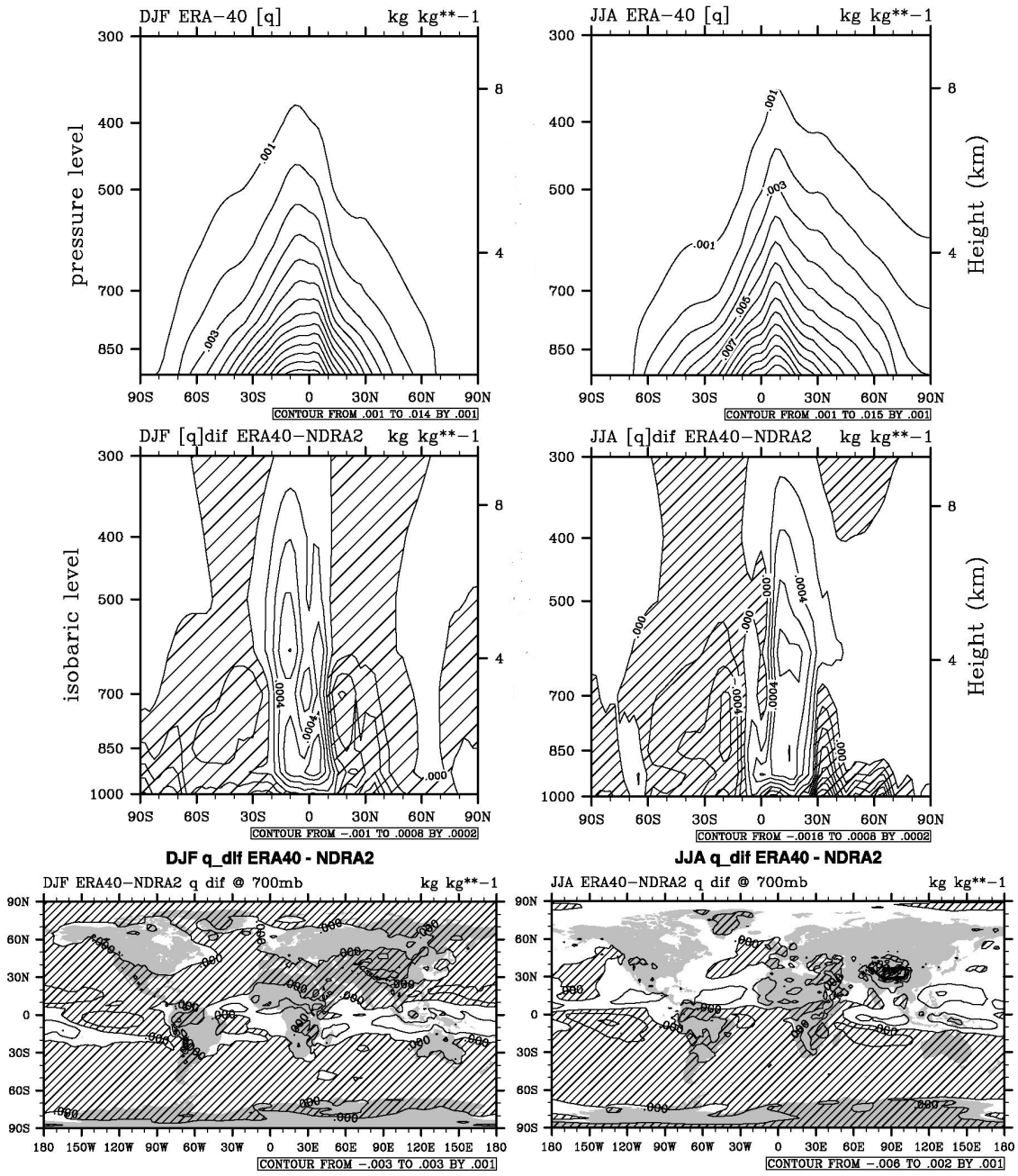

Fig. 11. Zonal mean specific humidity [q] ERA-40 data top row, [q] difference: ERA-40 minus NDRa2 middle row, bottom row is difference in q, ERA-40 minus NDRa2 at 700 hPa level. Left column DJF, right column JJA. Contour interval is 1 gm/kg for top and bottom rows, 0.2 gm/kg middle row. Negative values are shaded. Distribution of [q] for NDRa2 very similar in appearance to top row. ERA-40 has higher q than NDRa2 along most of the ICZ, lower in much of the winter hemisphere subtropics.

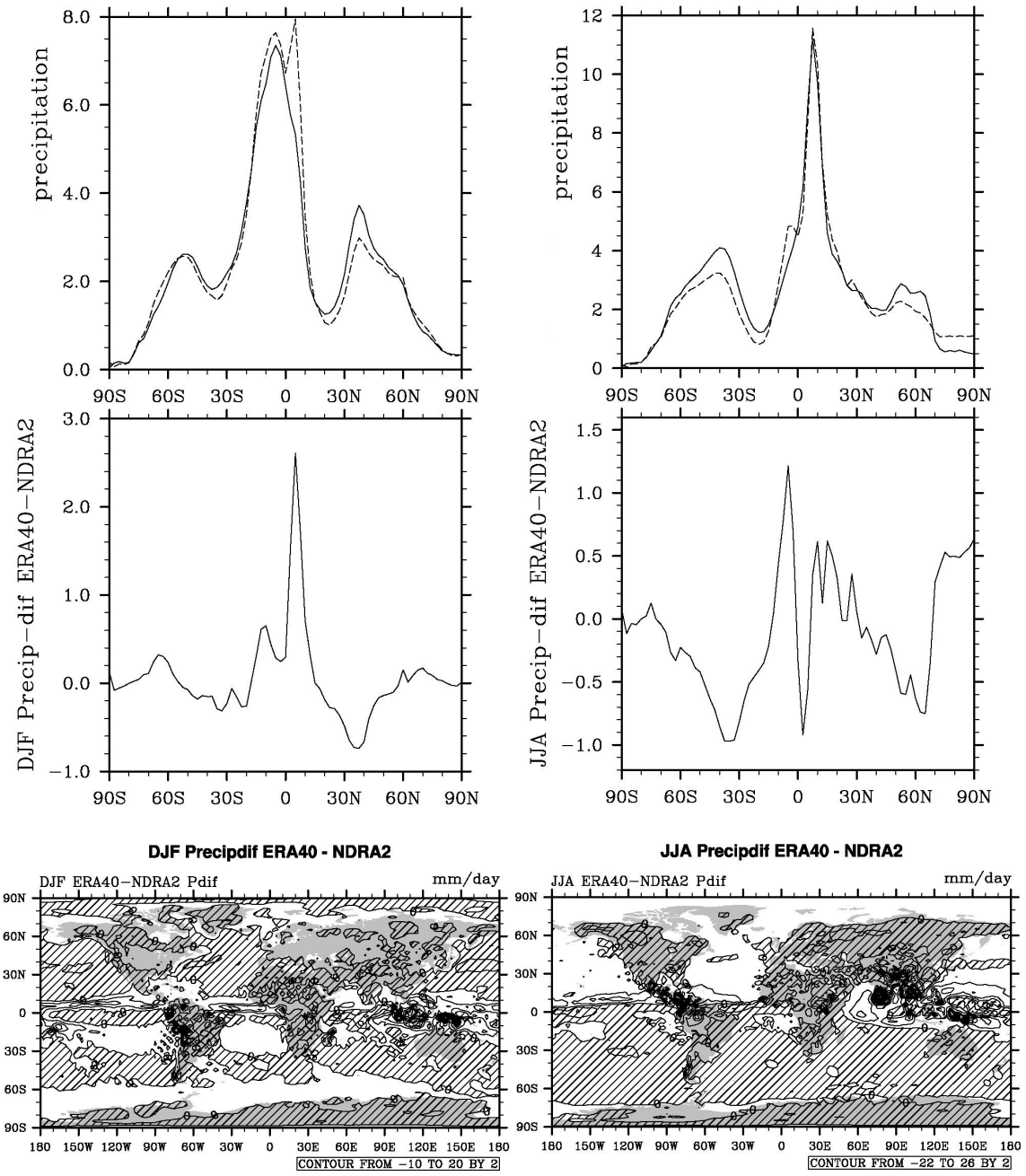

Fig. 12. Similar to fig. 1 except showing precipitation rate, P. Units are mm/day and the contour interval is 2 mm/day. ICZ in Atlantic and eastern Pacific has greater P in ERA-40.

In contrast, NDRa2 data has larger ICZ-associated P in Indian and west Pacific oceans. During winter, P in midlatitude storm tracks is generally less in ERA-40. During JJA, less P in ERA-40 over northern continents.

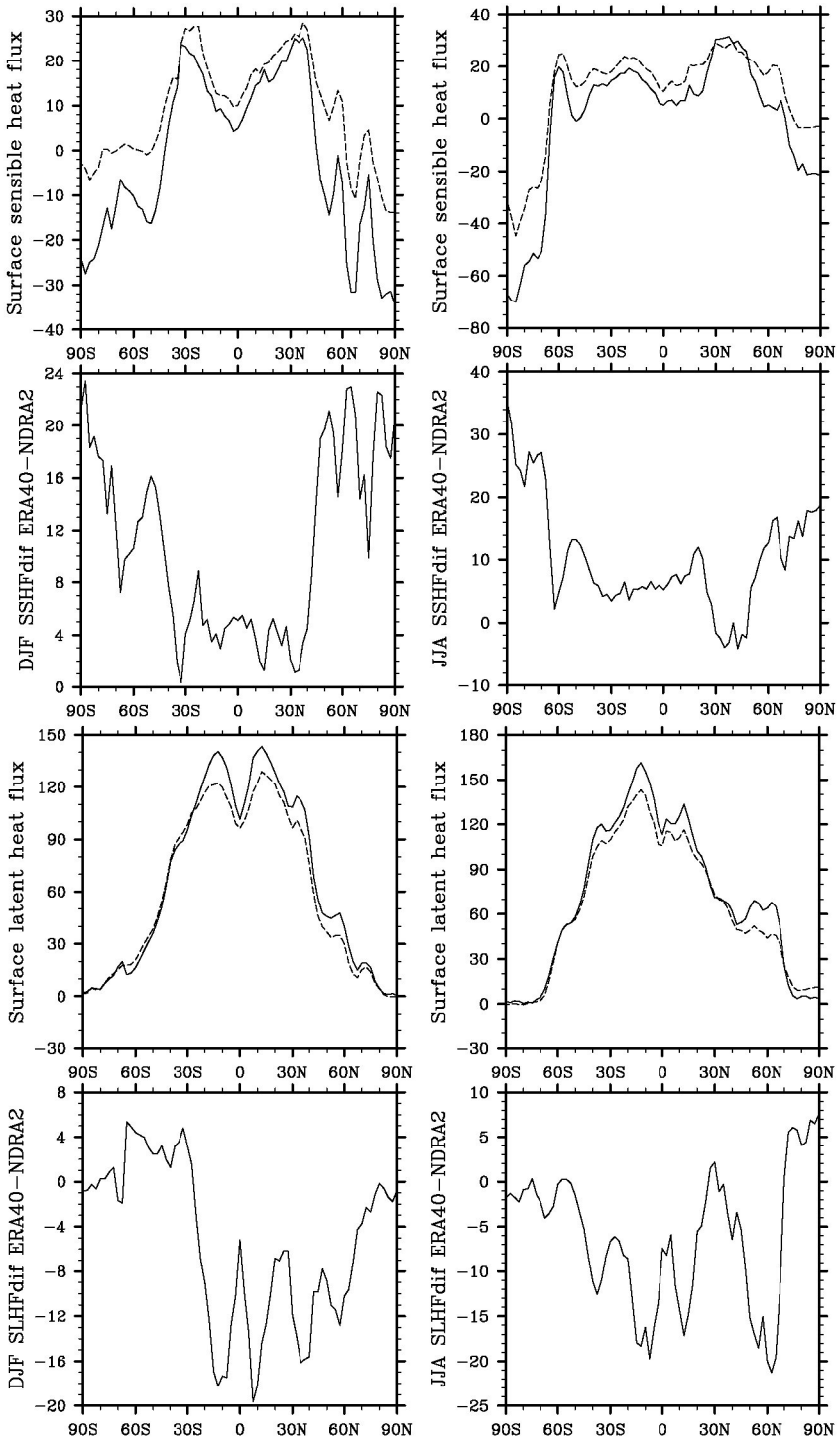

Fig. 13. Zonal mean surface sensible heat flux, [SHF] and ERA-40 minus NDRa2 difference (top and second row, respectively). Zonal mean surface latent heat flux, [LHF] and ERA-40 minus NDRa2 difference (third and bottom row, respectively). In top and third rows: solid line is NDRa2; dashed line is ERA-40. Units are W m^{-2}.

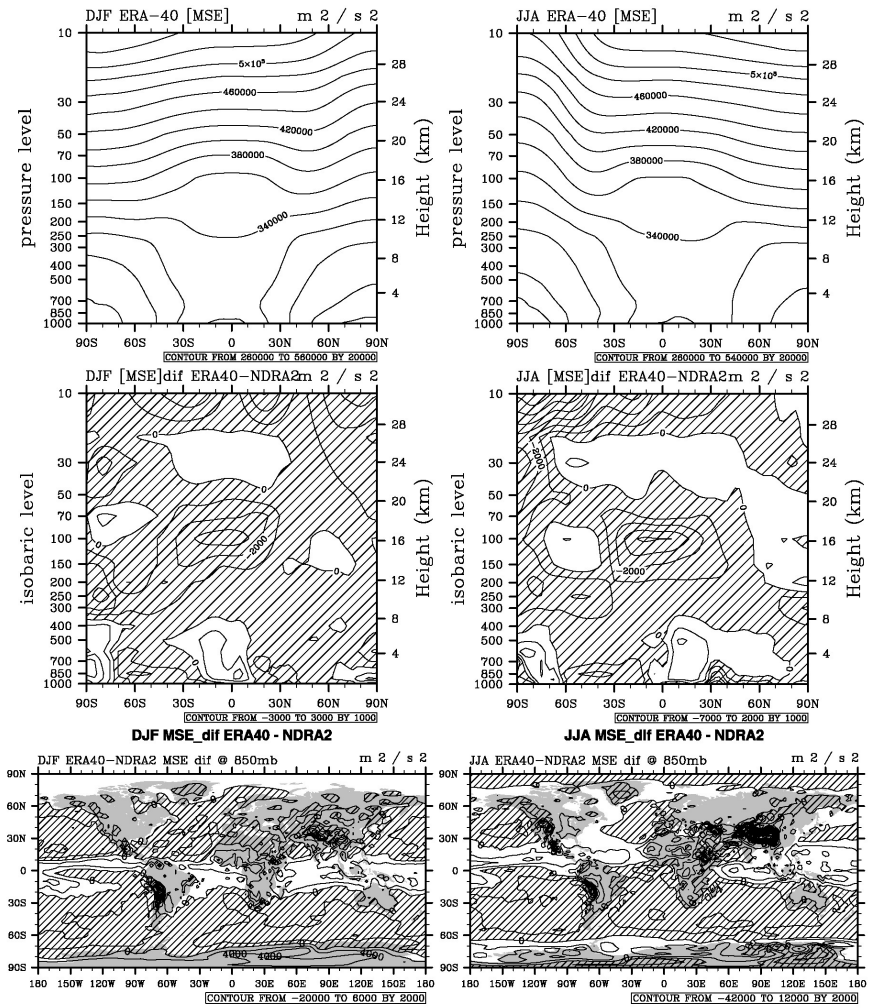

Fig. 14. Similar to fig. 5 except for moist static energy, MSE. Contour interval is 20 000 $m^2 s^{-2}$ for the top row and 1000 $m^2 s^{-2}$ for the middle row. The bottom row shows MSE at 850 hPa with contour interval 2000 $m^2 s^{-2}$. Low level tropical differences reflect greater moisture present in ERA-40 data, especially along the ICZ. Tropical tropopause and southern hemisphere low level midlatitudes regions differences reflect cooler ERA-40 temperatures there.

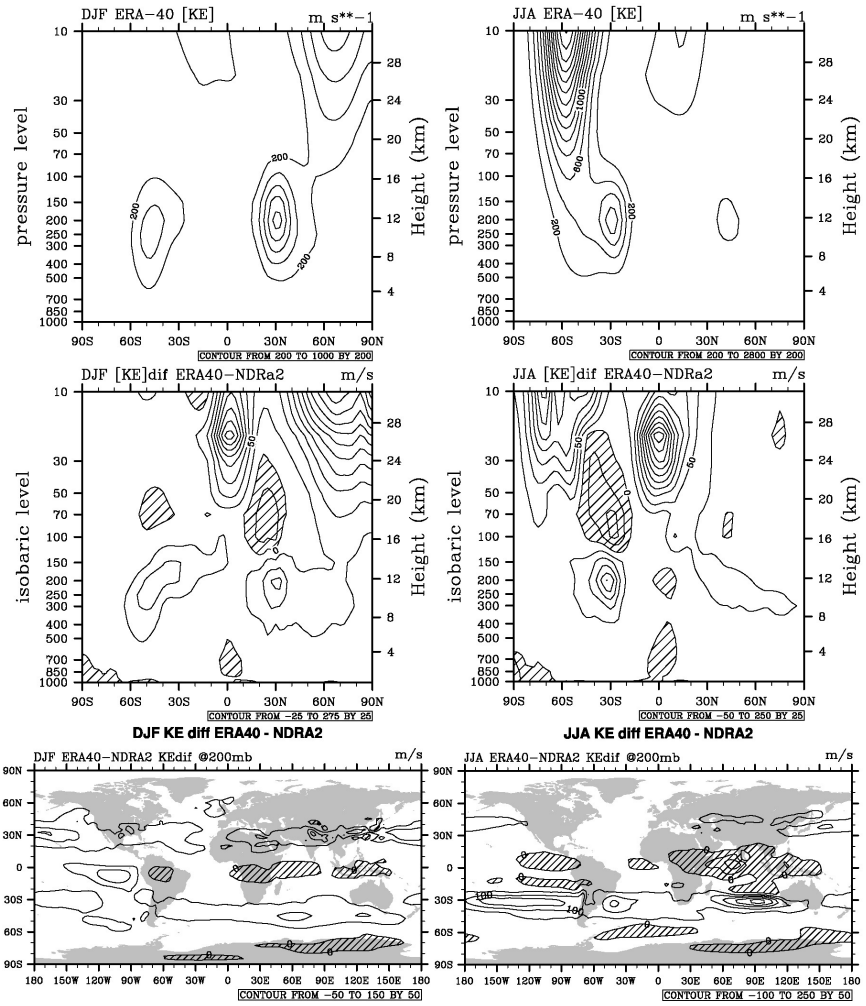

Fig. 15. Similar to fig. 5 except for kinetic energy, KE. Contour interval is 200 m^2 s^{-2} for the top row and 25 m^2 s^{-2} for the middle row. The bottom row shows KE at 200 hPa with contour interval 25 m^2 s^{-2}. ERA-40 data generally have more [KE] especially in winter stratosphere, winter subtropical jet, and tropical stratosphere.